Summertime Transport Pathways from Different Northern Hemisphere Regions into the Arctic

Cheng Zheng[1], Yutian Wu[1], Mingfang Ting[1], Clara Orbe[2], Xinyue Wang[3], and Simone Tilmes[3]

[1] Lamont-Doherty Earth Observatory, Columbia University, Palisades, NY, USA

[2] NASA Goddard Institute for Space Studies, New York, NY, USA

[3] Atmospheric Chemistry Observations and Modeling Laboratory, National Center for Atmospheric Research, Boulder, CO, USA

Corresponding author: Cheng Zheng (czheng@ldeo.columbia.edu)

Key Points:

- Identified fast, intermediate and slow transport pathways from various NH surface regions into the Arctic

- Midlatitude tracers are transported via the fast and intermediate pathways while low latitude tracers are transported by the slow pathway

- Analyzed and quantified dynamical processes, such as transient vs mean transport, associated with different pathways

20 **Abstract**

21   Trace gases and aerosols play an important role in Arctic chemistry and climate. As most

22 Arctic tracers and aerosols are transported from midlatitude source regions, long-range transport

23 into the Arctic is one of the key factors to understand the current and future states of Arctic

24 climate. While previous studies have investigated the airmass fraction and transit time

25 distribution in the Arctic, the actual transport pathways and their underlying dynamics and

26 efficiencies are yet to be understood. In this study, we implement a large ensemble of idealized

27 tagged pulse passive tracers in the Whole Atmosphere Community Climate Model version 5 to

28 identify and analyze summertime transport pathways from different Northern Hemisphere

29 surface regions into the Arctic.

30   Three different transport pathways are identified as those associated with fast,

31 intermediate and slow time scales. Midlatitude tracers can be transported into the Arctic in the

32 troposphere via the fast transport pathway (~8 days), which moves tracers northward from the

33 source region mainly through transient eddies. For the intermediate transport pathway, which

34 happens on 1~3 weeks' time scales, midlatitude tracers are first zonally transported by the jet

35 stream, and then advected northward into the Arctic over Alaska and northern North Atlantic.

36 Tropical and subtropical tracers are transported into the Arctic lower stratosphere via the slow

37 transport pathway (1~3 months), as the tracers are lifted upward into the tropical and subtropical

38 lower stratosphere, and then transported into the Arctic following the isentropic surfaces.

39

1 Introduction

The atmospheric composition of the Arctic, including trace gases and aerosols, has a substantial impact on Arctic climate and chemistry. Black carbon, which can be deposited onto ice and snow surfaces, or stay in the Arctic haze layer, increases the absorption of sunlight (e.g. Quinn et al., 2007; Warren and Wiscombe 1980). The climate forcing due to black carbon is suggested to be twice as large as that of carbon dioxide (Hansen and Nazarenko 2004) in the Arctic region. Longwave radiative transfer over the Arctic can also be modulated by direct and indirect aerosol effects, as the microphysical properties of clouds can be affected by aerosols (Garrett and Zhao 2006; Lubin and Vogelmann 2006; Coopman et al., 2018). The production of tropospheric ozone in the Arctic, which acts as a greenhouse gas, is related to halocarbons originating from midlatitudes (Atlas et al., 2003; Klonecki et al., 2003). Studies have shown that the amount of aerosols (including black carbon) and trace gases (e.g. ozone precursors) in the Arctic is largely contributed by transport from sources in the midlatitudes and the tropics (e.g. Klonecki et al., 2003; Bottenheim et al., 2004; Stohl 2006; Law and Stohl 2007; Fisher et al., 2010; Kupiszewski et al., 2013). Thus, it is important to understand the long-range transport from lower latitudes into the Arctic.

The distribution of aerosols and tracer species in the Arctic is determined by multiple factors including emissions, chemistry, transport and removal. The emissions, chemistry and removal processes differ for different species, making it difficult to understand the distribution of tracers. At the same time, understanding the transport processes, especially from different parts of the globe into the Arctic, can provide useful information about the contribution to Arctic air masses from different source regions. One way to isolate transport processes from emissions or chemistry is to implement idealized passive tracers into a model. The idealized tracers, which

63   have specified tracer removal time scales, are transported by the atmospheric flow in a model

64   without active chemistry involved. Therefore, these idealized tracers highlight the advective-

65   diffusive transport processes in the atmosphere, which are considered to be tracer-

66   independent (e.g., Holzer & Hall, 2000; Orbe et al., 2012).

67   Previous studies have explored transport pathways into the Arctic using idealized tracers.

68   Orbe et al., (2015a) investigated the Arctic airmass fractions using the Goddard Earth Observing

69   System Chemistry–Climate Model (GEOSCCM), in which they used tracers subject to steady

70   concentration boundary conditions over different regions in the planetary boundary layer (PBL)

71   and then integrated the model to reach a statistical equilibrium state. At equilibrium, the

72   concentrations of the tracers, therefore, reflected the fraction of air that last contacted the PBL in

73   different source regions. These so-called Arctic "airmass fractions" therefore represented the

74   relative contribution to Arctic tracer concentrations from different source regions. In particular,

75   they found that the airmass in the Arctic lower troposphere is dominated by air that last contacted

76   the PBL in the Arctic. By comparison, the air in the middle to upper troposphere of the Arctic

77   mostly originates from Northern Hemisphere (NH) midlatitudes, with the primary contribution

78   coming from the oceans during winter and from land during summer. Furthermore, they also

79   showed that the airmass in the Arctic upper troposphere and lower stratosphere (UTLS) mainly

80   originates from the tropics.

81   Using a related but distinct approach, Orbe et al., (2016) examined the transit-time

82   distribution (TTD), derived from idealized pulse tracers, corresponding to transport from

83   midlatitudes to the Arctic. Using the National Aeronautics and Space Administration (NASA)

84   Global Modeling Initiative (GMI) three-dimensional chemistry transport model (CTM), they

85   found that during boreal summer, tracer concentrations in the Arctic upper troposphere peak

86   around 10 days after the tracers are released, and the peak is around 30 days in the Arctic lower

87   troposphere. The TTD described in Orbe et al., (2016) and the airmass fraction analysis in Orbe

88   et al., (2015a) suggest that tracers released during summer in the midlatitudes are preferentially

89   drawn upward across isentropic surfaces within the midlatitudes before being transported toward

90   the Arctic approximately along the isentropes.

91   In this study, we focus on the summertime transport pathways into the Arctic by

92   analyzing a large ensemble of passive pulse tracers (100 tracers), which is much larger than the

93   four pulse tracers considered in Orbe et al. (2016), to achieve good statistics representing the

94   summertime transport. Other studies have also shown the summertime transport into the Arctic

95   and the impacts on Arctic climate using different approaches. For example, Laliberte and

96   Kushner (2014) found that summertime midlatitude moisture, which can be transported into the

97   Arctic, can explain a large part of the Arctic tropospheric temperature variability. Summertime

98   black carbon concentrations over the Arctic, which mostly come from source regions at lower

99   latitudes (e.g. Xu et al., 2017; Liu et al., 2015), can also have large impacts on radiative balance,

100   which leads to increased warming in the Arctic (e.g. Bond et al., 2013; Hansen and Nazarenko

101   2004). In addition, studies have also linked the Asian summer monsoon circulation to the climate

102   and chemistry of the Arctic. Krishnamurti et al. (2015) examined a case study and argued that the

103   moisture outflow associated with the Asian summer monsoon circulation caused a rapid melting

104   of the Arctic sea ice during various monsoon heavy rainfall events in 2006-2012. Liu et al.,

105   (2003) also found that variability in the monsoon can lead to the variations in pollution transport

106   into the Arctic. However, the role of the summer monsoon circulation on the Arctic transport is

107   not well established. Note that the idealized tracers in our study, which have a spatially uniform

108   source, are different from realistic tracer species that usually have large spatial variations in

109   terms of their source or emission. Our approach with idealized tracers is to focus on the transport

110   pathway, i.e. how the idealized tracers are transported into the Arctic and what atmospheric

111   circulation processes are involved. To attribute the Arctic concentration of any realistic chemical

112   species to different source regions, an approach considering the spatial variation of the source

113   distribution is required.

114   Several questions warrant further study in terms of summertime transport into the Arctic.

115   First, what are the similarities and differences in transport pathways and timescales among

116   different regions in the midlatitudes and the tropics? What are the physical processes involved in

117   transporting tracers from the tropics and midlatitudes into the Arctic? As pointed out by Orbe et

118   al., (2016), midlatitude tracers are preferentially lifted upward and then transported poleward

119   during summer. To this end, we ask here: a) What are the processes that lift up the tracers? By

120   convection or large-scale rising motion? b) What are the processes that transport the tracers

121   northward into the Arctic? What is the relative importance of transient eddies and the mean

122   atmospheric circulation? c) How do the timescales and processes differ for different midlatitude

123   regions? These questions will be the focus of this study. The model experimental design and

124   diagnostic methods will be introduced in section 2. The evolution of tracer distribution in the

125   Arctic will be discussed in section 3. Different transport pathways, as well as the atmospheric

126   circulations involved, will be explored in section 4. Discussions and conclusions will be

127   presented in section 5.

128

129   **2 Methods**

130   2.1 Model Simulations

131   The Whole Atmosphere Community Climate Model version 5 (WACCM5) is used in this

132   study. WACCM5 is the high-top atmospheric component of the Community Earth System Model

133   version 1 (CESM1; Hurrell et al., 2013). The WACCM5 used here has 110 vertical levels with a

134   horizontal resolution of 0.9° latitude and 1.25° longitude. The model physics for WACCM5 is

135   the same as the Community Atmospheric Model version 5 (CAM5) (Neale et al., 2010), with the

136   shallow convection scheme from Park and Bretherton (2009) and deep convection scheme

137   developed by Zhang and McFarlane (1995). We integrate the model with prescribed historical

138   sea surface temperatures and sea ice concentrations from January 1981 to December 1991.

139   The 110 vertical levels in WACCM5 greatly improve the vertical resolution from mid-

140   troposphere to lower stratosphere (Garcia and Richter, 2019). The high vertical resolution helps

141   to better simulate the temperature, wind and water vapor distribution in the UTLS (Wang et al.,

142   2018). Wu et al., (2020) used a similar setup of WACCM5 and found that the Asian summer

143   monsoon region is favorable for fast transport of tracers from the surface into the UTLS. Thus,

144   the 110-layer WACCM5 can be beneficial for understanding the tracer transport within the

145   UTLS and from Asian summer monsoon region to the Arctic (e.g. Ikeda et al., 2017; Koch and

146   Hansen 2005).

147   2.2 Idealized Tracers

148   The idealized tracers imposed in the model are similar to that in Wu et al., (2020). Here

149   we use the "Boundary Impulse Response (BIR)", or simply "pulse" tracer approach (Holzer et

150   al., 2000; Haine et al., 2008). The BIR can be interpreted as the time-evolving response

151    $G(r, t|\Omega, t')$ at a location r and time t to a pulse of a conserved and passive tracer which is

152   released in the source region Ω at time t'. BIR is tracer-independent as it does not involve any

153   chemical processes or interior sources/sinks (e.g., Holzer and Hall, 2000; Orbe et al., 2012).

154   Therefore, the BIR provides a direct measure of transport properties from source regions into the

155   Arctic, which isolates the transport from chemistry processes. This approach has been used to

156   examine seasonal variations in stratospheric age spectra (Li et al., 2012; Ploeger and Birner,

157   2016), transport from the NH midlatitude surface to different regions around the globe (Orbe et

158   al., 2016), as well as transport from NH surface to UTLS (Wu et al., 2020). Note that the BIR

159   can be used to construct the TTD, which is one approach used in previous studies (Holzer &

160   Hall, 2000; Li et al., 2012; Orbe et al., 2016) to measure the transit time at r independent of

161   when (with respect to t') the tracer was last at the Earth's surface. Similar to Wu et al., (2020),

162   our focus here is on quantifying how the tracer distribution at time t and location r is related to

163   tracer source Ω conditioned on its release time.

164   Idealized pulse tracers are imposed in WACCM5 over different NH surface regions. The

165   regions are shown in Figure 1a. There are 5 NH midlatitude regions, including Asia (ASI),

166   Pacific (PAC), North America (NAM), Atlantic (ATL) and Europe (EUR). The northern

167   boundary of these regions is located at 60°N and the southern boundaries range from 20° to

168   25°N, which are similar to that in Orbe et al., (2015a). In addition, to highlight the role of the

169   Asian summer monsoon, we also tagged tracers that are released over the Tibetan Plateau (TP)

170   and North India (NI). Tracers that are released to the south of these regions in NH are tagged as

171   Tropics (TR). Note that although we also release tracers north of 60°N, we will not include this

172   case here as our focus is on long-range transport pathways into the Arctic. Tracers are released

173   uniformly at each source region during the first day. The tracer concentration is set to 1 mol/mol

174   at the surface during the first 24 hours within the source region, while outside the source region

175   the boundary concentration is set to 0. The tracers are transported freely in the atmosphere with

176   no loss as long as they do not touch the surface. The tracer concentration is set to 0 whenever

177   they are in contact with the surface after the first day. The transport of pulse tracers into the

178   Arctic, which can happen on relatively short time scales, likely have a high dependency on

179   meteorology. Thus, large variability in the transport is expected from tracer to tracer when they

180   are released at different times. To achieve more robust results, a large ensemble of tracers is

181   implemented in the model. A total of 10 tracers are released each summer, on days 3, 10, 17, 24,

182   and 31 in July and August, and repeated for all 10 summer seasons, 1981–1990. Therefore, we

183   have a total of 100 tracers for each source region. The choice of 100 tracers for each source

184   region is a compromise between maximizing the number of tracer ensembles and the

185   computational costs of the model experiments. Model outputs of daily means of meteorological

186   fields, as well as tracer concentrations and budget terms, are saved for further analysis.

187   Compared to Orbe et al., (2016), with a much larger number of tracers (100 vs 4) and multiple

188   midlatitude regions, the methods used in this study can provide information that potentially links

189   the Arctic tracer concentration to different NH source regions, as well as decomposes the

190   transport into transients and time-mean components (see section 2.3).

191   2.3 Diagnostics of Tracer Transport

192   The daily model output is interpolated to 28 pressure levels from 1000 to 50hPa prior to

193   any analysis. The intervals among the pressure levels are 50hPa from 1000 to 300hPa, 25hPa

194   from 300 to 100hPa, and 10hPa from 100 to 50hPa. As in Wu et al., (2020), the tracer budget can

195   be written as the contribution from different processes:

196
$$\frac{\partial \chi}{\partial t} = RD + VD + COND + CONS \qquad (1),$$

197   where χ is the concentration of the pulse tracer. RD, VD, $COND$, and $CONS$ are the tracer

198   tendencies due to transport by model's resolved dynamics, vertical diffusion, deep convection

199   and shallow convection, respectively. The tracer concentration χ, as well as the four terms on the

200   rhs of (1) are all taken from the direct model outputs. Wu et al., (2020) showed that equation (1)

201   is well balanced by using the model outputs, and the balance is also well maintained after the

202   data is interpolated onto pressure levels (not shown). The transport of the tracers by resolved

203   dynamics RD is simply the advection of the tracers by the model's (resolved) circulation:

204   $$RD = -\vec{U} \cdot \nabla \chi \qquad (2),$$

205   where $\vec{U}$ is the three-dimensional wind vector. In the pressure coordinates, as the divergence of

206   the three-dimensional wind is zero ($\nabla \cdot \vec{U} = 0$), (2) can be written as:

207   $$RD = -\nabla (\vec{U} \cdot \chi) \qquad (3),$$

208   or,

209   $$RD = -\frac{\partial(u \cdot \chi)}{\partial x} - \frac{\partial(v \cdot \chi)}{\partial y} - \frac{\partial(\omega \cdot \chi)}{\partial p} \qquad (4),$$

210   where u, v, and ω are zonal, meridional and vertical motion in pressure coordinates. Therefore,

211   the tracer tendency due to resolved dynamics equals the convergence of the three-dimensional

212   tracer flux by the resolved atmospheric circulation. As daily χ, u, v, and ω are available, we can

213   compute the contributions of tracer tendency by resolved dynamics in the zonal, meridional and

214   vertical directions explicitly. Note that model output RD is calculated on the model grid (hybrid

215   vertical levels) at each model time step, while we estimate each term on the rhs of equation (4)

216   by using daily mean values on pressure levels. Therefore, the estimation using the rhs of

217   equation (4) may contain some errors, which will be discussed in section 4.

218   When computing the tracer tendency using equations (1) and (4), we will only show the

219   results for the ensemble mean of tracers, as tracer to tracer variability is not the focus of this

220   study. However, tracer to tracer variability can provide information regarding the contributions

221   from time-mean and transient flows. We analyze the variability from tracer to tracer by

222   considering the time series of the tracer concentration. Given N number of tracers that are

223   released at $t' = t_1', t_2', \ldots, t_N'$ and at source region Ω, the tracer concentration of one particular

224   tracer (n) at location r at a fixed transit time (number of days after the tracers are released) $\xi =$

225    $t - t'$ (where t is the current time when the tracer concentration is observed) can be written as:

226                             $$\chi(n, \xi, \Omega, r)$$

227   where $n = 1,2, \ldots, N$. As t' is only a function of n, and time $t = \xi + t'$, for fixed transit time ξ, t

228   and n is an injective function (one-to-one function). So, $\chi(n, \xi, \Omega, r)$ can also be written as.

229                             $$\chi(t(n, \xi), \xi, \Omega, r)$$

230   which can be considered as a time series. Note that the method here to consider an ensemble of

231   pulse tracers that are released at different time as a time series at fixed transit time ξ, is the same

232   as the method used in Holzer et al., (2003). This time series can be decomposed into the time

233   mean (averaging over t) and the deviation from time mean:

234            $$\chi(t(n, \xi), \xi, \Omega, \boldsymbol{r}) = \bar{\chi}(\xi, \Omega, \boldsymbol{r}) + \chi'(t(n, \xi), \xi, \Omega, \boldsymbol{r})$$

235   here the overbar denotes the time mean, and prime denotes the deviation from the time mean.

236   Again, for fixed transit time ξ, t and n is an injective function (one-to-one function), so

237   averaging over t is equivalent to averaging over n. Thus, the time mean $\bar{\chi}(\xi, \Omega, \boldsymbol{r})$ is equivalent

238   to ensemble mean of tracers at fixed ξ.

239   Similarly, the time series of circulation variables, such as the meridional wind $v(t, r)$ can also be

240   decomposed in a similar way:

241                      $$v(t(n, \xi), \boldsymbol{r}) = \bar{v}(\xi, \boldsymbol{r}) + v'(t(n, \xi), \boldsymbol{r})$$

242   To match the form of tracer concentration, both the time-mean meridional wind and the

243   deviation from time mean also depend on transit time ξ. Thus we can write the time mean of the

244   meridional flux of tracers as

245    $$\overline{v \cdot \chi} = \bar{v}\,\bar{\chi} + \overline{v'\chi'} \quad (5),$$

246   where the first term on the rhs of (5) is the transport by time-mean meridional wind (including

247   both zonal mean meridional circulation and stationary waves), and the second term represents the

248   transport by transients that includes all time scales shorter than the time mean.

249   Similar to equation (5), the vertical flux of the tracer transport by resolved dynamics can

250   be decomposed as:

251    $$\overline{\omega \cdot \chi} = \bar{\omega}\,\bar{\chi} + \overline{\omega'\chi'} \quad (6),$$

252   to evaluate the relative contribution from time-mean and transient components.

253   The analysis in this study will only focus on the ensemble mean of 100 tracers for each

254   source region, which are released during July and August in 10 years. That means we only

255   investigate the transport pathways in terms of climatological mean. Different transport pathways

256   can have subseasonal, interannual and decadal variabilities, which are beyond the scope of this

257   study and will be explored in the future.

258

259   **3 Temporal Evolution of Tracer Concentration in the Arctic**

260   We focus on the tracer concentration in the Arctic, which is defined as the region north of

261   70°N. When the pulse tracers are released, sharp horizontal gradients of tracer concentration are

262   created at the boundaries of the tracer source regions (e.g., the northern boundary of midlatitude

263   source regions at 60°N in Fig. 1a). These sharp gradients can lead to artificially strong horizontal

264   transport of tracers locally due to diffusion or mixing (also see section 4.2). Thus, the southern

265   boundary of the Arctic is defined as 70°N, away from the northern boundary of the source

266   regions (60°N). The time evolution of tracer concentration for lower-to-mid troposphere (1000-

267   600 hPa), mid-to-upper troposphere (600-200 hPa), and lower stratosphere (200-100 hPa) over

268   the Arctic is shown in Figures 1b-d respectively. Each color denotes the contribution from one

269   source region. The total tracer concentration from all source regions peaks at about 10 days in

270   the troposphere (Figs. 1b, c), but at around 100 to 120 days in the lower stratosphere (Figure 1d).

271   In the troposphere, most of the Arctic tracers originate from the 5 midlatitude regions: ASI, PAC,

272   NAM, ATL and EUR on relatively short time scales. Tracers from the tropics only contribute

273   significantly after days 20-30 from the day the tracers are released. In the lower stratosphere,

274   most of the contribution to the Arctic tracer concentration is from the tropics, as well as TP and

275   NI tracers, with ASI tracers having the largest contribution among the 5 midlatitude regions. The

276   Asian summer monsoon regions (TP and NI), which cover a relatively small area compared to

277   the tropical region TR (Figure 1a), have significant contributions to the tracer concentration in

278   the Arctic lower stratosphere (Figure 1d), showing that TP and NI tracers are transported into the

279   Arctic lower stratosphere very efficiently. Note that, these findings are consistent with the results

280   in Orbe et al., (2015a), in that most of the tracer concentration over the Arctic troposphere

281   originates from the midlatitudes, whereas the tropics has the largest contribution to the tracer

282   concentration in the Arctic lower stratosphere. However, our results cannot be quantitatively

283   compared to Orbe et al., (2015a) as the tracers are removed when they come in contact with the

284   surface after day 1, whereas tracers are retagged in Orbe et al., (2015a) when they touch the

285   surface. In addition, since a large number of tracers are removed at the surface (see section 4.2),

286   only a small portion of the tracers are transported into the Arctic. As tracer species and aerosols

287   are not necessarily removed when they touch the surface in the real atmosphere, it is not very

288   meaningful to quantify the exact tracer fraction that are transported into the Arctic in our

289   experiment.

290   As the areas covered by different source regions differ, to better compare the efficiency

291   of the tracer transport from different regions, we normalized the tracer concentration by the area

292   of the source region. The normalized tracer concentration, which is measured by the Arctic tracer

293   concentration (ppbv) per unit area of source region (square kilometer), is shown in Figs. 1e-g.

294   Among the 5 midlatitude regions (ASI, PAC, NAM, ATL and EUR) that have most of the

295   contributions to the Arctic tracer concentration in the troposphere, ATL, EUR and NAM tracers

296   have sharp peaks with fast growth and decay: ATL and EUR tracers peak at around 6-9 days in

297   both lower and upper troposphere while NAM tracers at about 10 days. In comparison, ASI and

298   PAC tracers have flat peaks. Both ASI and PAC tracer concentration stays in high value during

299   day 10-20 in mid-to-upper troposphere (Figure 1f). ASI tracer concentration slowly increases

300   during day 10-30 in the lower troposphere, while PAC tracer concentration slowly decreases

301   during day 10-20 (Figure 1e). The growth rate of the tracer concentrations in the Arctic

302   troposphere (the slope of the normalized concentrations in Figure 1e-f) is the largest during the

303   first 6-8 days for ASI, PAC, ATL and EUR tracers, indicating that similar dynamical processes

304   are likely at play on the short timescales in these regions. We name this the fast transport

305   pathway. From days 8 to 20, the tracer concentrations tend to maintain at high values in the mid-

306   to-upper troposphere for ASI and PAC tracers (Figure 1e, f). This will be referred to as the

307   intermediate transport pathway with a timescale of about 1-3 weeks. For NAM tracers, the peak

308   time is about 10 days, which is shorter than ASI and PAC and longer than EUR and ATL. Later

14

309   on, we will show that this is likely due to the combination of the fast and intermediate transport

310   pathways.

311   For the Arctic lower stratosphere, although TR has the largest contribution to the total

312   concentration (Figure 1d), NI and TP tracers are more efficiently transported into the Arctic

313   when normalized by the surface areas, compared to other regions, with a peak time around 90-

314   100 days (Figure 1g). The growth rate of the NI and TP tracers becomes large at about 20 days

315   after the tracers are released. This indicates the important role the Asian summer monsoon plays

316   in tracer transport into the Arctic lower stratosphere (Orbe et al., 2015b). ASI and TR tracers are

317   also transported into the Arctic on the 100-day to 150-day time scales, while the transports from

318   ATL, PAC, EUR, and NAM are negligible on the long time scales. It is interesting to note that

319   the 100-day time scale is much longer than that within the troposphere (Figure 1e-f). This will be

320   termed as the slow transport pathway in the rest of the study.

321   The three different transport pathways noted above, with fast (~1 week), intermediate

322   (1~3 weeks) and slow (1~3 months) time scales, are defined by analyzing the evolution of the

323   passive tracer concentration reaching the Arctic. In the real atmosphere, different tracer species

324   have different lifetimes. For example, the lifetime of butane is about 1 week, propane has a

325   lifetime of about 2 weeks, and ethane and carbon monoxide have averaged lifetimes of

326   approximately 2 months. Thus, the three transport pathways may play different roles in

327   transporting different tracer species. For example, the slow transport pathway may have little

328   contribution to short-lived species like butane and propane; while the fast transport pathway may

329   be relevant for tracer species of both short and long lifetimes. Note that these examples are just

330   used to illustrate that different pathways can be potentially important for different tracer species.

331   However, as our experimental design does not consider tracer loss via certain processes (e.g. wet

332   deposition, which can happen when tracer species are rained out), as such, it cannot completely

333   address the question of the relevance of different transport pathways for any specific tracer

334   species. In the following sections, we will explore the dynamical processes contributing to each

335   of the three transport pathways by using actual concentration of the tracer (not normalized

336   concentration).

337

338   **4 Tracer Transport Pathways into the Arctic**

339   4.1 The Role of Meridional Tracer Flux

340   Before going into details of the different transport pathways, we first consider the budget

341   of the tracer concentration integrated over all grid points in the Arctic ($\iiint_{arctic} \chi$), from the

342   surface to the top of the atmosphere and from 70°N to the north pole. Using tracer mass

343   conservation, one can show that the budget of the total Arctic tracer concentration ($\iiint_{arctic} \chi$)

344   can be written as:

345   $$\frac{\partial}{\partial t} \iiint_{arctic} \chi dV = \oiint_{70N} v \cdot \chi + (removal\ of\ tracer\ at\ Arctic\ surface) \qquad (7).$$

346   Thus, the only way tracers can be transported into the Arctic from the midlatitudes or tropics is

347   through the poleward flux at the southern boundary, i.e. 70°N. The temporal and spatial

348   distribution of the meridional flux can thus determine the evolution of the tracer concentration

349   within the Arctic. To illustrate this, we show the vertically (1000-100 hPa) and zonally averaged

350   meridional flux of the five midlatitude regions (ASI, PAC, NAM, ATL and EUR,) in Figure 2 a-

351   e. The strongest poleward flux at 70°N (dark green dashed line) is within the first 8 days for all

352   five regions. This is consistent with the largest growth rate of tracer concentration during the first

353   8 days in Figure 1 e-f (the fast transport pathway; see section 3), as implied by equation (7). The

354   meridional flux shifts to negative (black line indicates the zero line) after about day 7-9 for ATL

355   and EUR tracers, corresponding to the decrease of tracer concentration after 7-9 days (Figure 1e-

356   f); the meridional flux stays positive with a small amplitude from about day 8 to 20 for ASI and

357   PAC tracers, which is also consistent with the tracer evolution during that period of time (Figure

358   1e-f; the intermediate transport pathway). In addition, the meridional tracer flux shifts to

359   negative at around day 10 for NAM tracers, which coincides with the timing of the peak tracer

360   concentration of NAM tracers (Figure 1e-f). Therefore, the key to explain the tracer evolution

361   within the Arctic is to understand the spatial and temporal structure of the meridional tracer

362   fluxes, which will be the main focus in the following discussions about the fast and intermediate

363   transport pathways.

364   4.2 The Fast Transport Pathway

365   As discussed above, the meridional tracer flux is large during the first 8 days after the

366   tracers are released for all the midlatitude source regions. We show in Figure 2f-j the spatial

367   structure of the vertically integrated meridional tracer flux (shading in Figure 2) for ASI, PAC,

368   NAM, ATL and EUR,. The vertically integrated tracer concentrations, denoted by the black

369   contours, show the highest concentration located near where the tracers are released. Northward

370   flux into the Arctic is located in regions directly to the north of each source region. This indicates

371   that the fast transport pathway is mostly due to direct northward transport from the source region

372   into the Arctic by the atmospheric circulation.

373   To determine the vertical structure of the meridional transport, Figure 3 shows the

374   zonally averaged tracer concentration and meridional flux over the local area outlined by the

375   dark green lines as in Figure 2 for each region. These cross sections are plotted for days 1-2, 3-5

376   and 6-8 after the tracers are released for ASI, PAC, NAM, ATL and EUR tracers to better

377   illustrate the temporal evolution.

378   There are some similarities among the cross sections for tracers released in different

379   midlatitude regions. During day 1-2 (first column in Figure 3), strong northward transport can be

380   found near 60°N in the lower troposphere among all regions. As the northern boundary of the

381   tracer source regions is at 60°N, a strong meridional gradient of tracer concentration appears

382   immediately after the tracers are released. The maximum northward flux of tracers at 60°N in the

383   lower troposphere is expected (first column in Figure 3 and first column in Figure 2). In addition,

384   the northward transport in the upper troposphere is broader and weaker compared to the lower

385   troposphere during day 1-2. The tracer concentration (black contours) is higher in the lower

386   troposphere than in the upper troposphere, but a small amount of tracers have already been lifted

387   up into the upper troposphere during day 1-2. During day 3-5 (second column in Figure 3),

388   compared with day 1-2, the northward flux extends northward, with large northward transport in

389   both upper and lower troposphere. Although the tracer concentration generally decreases during

390   day 3-5 due to the surface removal process, the concentration is more evenly spread out in the

391   vertical, indicating further lifting of lower tropospheric tracers into the upper troposphere. Both

392   the tracer concentration and the northward flux become weaker during day 6-8 (third column in

393   Figure 3).

394   The northward flux going into the Arctic is the strongest during day 3-5, with strong

395   transport in both the upper and lower troposphere among all 5 regions. The question is what

396   processes are responsible for the upward tracer transport from the surface into the lower and

397   upper troposphere. We apply the tracer budget analysis as in Eqs. 1 and 4 to address this

398   question. The different terms on the right side of Eq. 1 are shown in Figure 4 averaged for 30°-

399   70°N region as in Figure 3, for the upper (200-500 hPa; first column) and lower troposphere

400   (500-950hPa; second column). Following Eq. (1), the tendency of the tracers can be separated

401   into contribution from deep convection ($COND$; red), shallow convection ($CONS$; orange),

402   vertical diffusion (VD; blue) and resolved dynamics (RD; green). With equation (4), the resolved

403   dynamics term can be further decomposed into transport by zonal wind (purple), meridional

404   wind (magenta) and vertical velocity (cyan). The three-dimensional decomposition of the

405   transport by resolved dynamics is crosshatched to distinguish them from the 4 terms in equation

406   (1). The sum of the three-dimensional convergence components is approximately equal to the

407   resolved dynamics term, as the residual (yellow shadings) is generally small. Note that the results

408   for all 5 midlatitude regions are qualitatively similar in Figure 4. During days 1-2 in the upper

409   levels (Figure 4a), deep convection (red) has the largest contribution. There is also significant

410   contribution from resolved dynamics (green), which mostly comes from the vertical transport

411   (crosshatched cyan). For days 3-5 in the upper troposphere (Figure 4c), there is little contribution

412   by diffusion or convection processes ($COND$, $CONS$, and VD). Instead there is a large positive

413   tracer tendency due to vertical transport by resolved dynamics, while at the same time, the

414   tracers are also transported out of the region by zonal and meridional fluxes. For days 6-8, the

415   tracer tendency in the upper levels is mostly from the zonal transport, which is transported

416   downstream out of the averaging region. In summary, tracers are transported into the upper

417   troposphere mostly by deep convection and resolved dynamics (specifically, vertical fluxes). If

418   we combine the contribution during both day 1-2 and 3-5, the net effect of vertical transport by

419   resolved dynamics is comparable to the contribution by deep convection in all 5 regions.

420   In the lower troposphere (second column in Figure 4), vertical diffusion contributes the

421   most, while deep and shallow convections have little contribution. Since the tracers are released

422   during day 1, the tracer concentration is high near the surface, creating a strong vertical gradient

423   in tracer concentrations and thus vertical diffusion can effectively bring the tracers up from the

424   surface to the lower troposphere during day 1-2 (Figure 4b). As the tracer concentration

425   decreases at the surface after day 1, the vertical gradient of tracer concentration reverses, and

426   vertical diffusion brings the tracers downward back to the surface (Figure 4d). Since deep

427   convection can bring tracers from the surface up into the lower troposphere (net gain of tracer

428   concentration in the lower troposphere), and also lift tracers from the lower troposphere into the

429   upper troposphere (net loss of tracer concentration in the lower troposphere), it plays little role in

430   the lower troposphere (Figure 4b and d). Shallow convection vertically redistributes the tracers

431   within the lower troposphere. This vertical redistribution has little net contribution to the tracer

432   concentration when averaged within the lower troposphere (500-950 hPa; Figure 4b, d, and f).

433   Also note that when the tracers are released on day 1, a large vertical gradient of tracer

434   concentration is created near the surface, which leads to a large upward flux due to the vertical

435   motion near the surface. This is the reason that the vertical transport by large-scale ascent leads

436   to a positive tracer tendency in both upper troposphere (Figure 4a) and lower troposphere (Figure

437   4b).

438   To explore the relative contributions of the time-mean and transient circulation to the

439   meridional and vertical fluxes, we use equations (5) and (6) to further decompose these fluxes.

440   We analyze the meridional tracer flux averaged over 50°-70°N within the cross sections in

441   Figure 3 for all 5 midlatitude regions. Note that generally the strongest meridional flux is located

442   between 50°and 70°N (Figure 3), and the meridional flux at this latitude band is likely to

443   contribute to the transport into the Arctic. Also, though here the analysis is within the entire

444   troposphere (200-950 hPa), we reach similar conclusions regarding the time-mean and transient

445   transport if upper and lower troposphere are analyzed separately (not shown). Note that, as

446   transient wind is defined as deviation from time-mean wind during 10 years in equations (5) and

447   (6), transient transport includes contribution from variability on all different time scales

448   (interannual, month-to-month, sub-monthly). Our analysis shows that the transient transport is

449   dominated by contribution from short time scale variability (sub-monthly; not shown).The

450   decomposition of meridional flux (first column in Figure 5) shows that, consistently over the first

451   8 days, most of the northward flux is due to transients (blue) for EUR, ASI and NAM tracers,

452   while transport by time-mean wind (orange) and transients are both important for ATL and PAC

453   tracers. The transport by time-mean wind, which is likely due to the northward transport near the

454   exit of the Pacific and Atlantic jet, will be discussed in more detail in section 4.3. The

455   decomposition of vertical flux by resolved dynamics (second column in Figure 5), shows that

456   transients (cyan) are important for tracers released in all 5 regions, with the time-mean vertical

457   transport (green) also making a large contribution for ASI and NAM tracers.

458   In short, the fast transport pathway brings midlatitude tracers directly into the Arctic in

459   both the lower and the upper troposphere within about 8 days. Vertical diffusion brings tracers

460   up into the lower troposphere, while deep convection and resolved dynamics bring tracers into

461   the upper troposphere. The poleward transport of the tracers into the Arctic is dominated by

462   transients for Asian, European and North American tracers, while both time-mean and transient

463   transports are important for poleward transport of Pacific and the Atlantic tracers.

464   4.3 The Intermediate Transport Pathway

465   Now we investigate what circulation processes contribute to the intermediate time scale

466   transport pathway. As discussed in section 3 and 4.1, during day 9-20 after the tracers are

467   released, the meridional tracer flux continues transporting ASI and PAC tracers into the Arctic

468   substantially, which maintains or slightly increases the ASI and PAC tracer concentrations in the

469   Arctic. On the contrary, the meridional tracer flux becomes southward for EUR and ATL tracers.

470   To understand this, in Figure 6a-e, the day 9-20 vertically integrated (1000-100hPa) meridional

471   tracer flux (shadings) for ASI, PAC, NAM, ATL, and EUR tracers is shown respectively. The

472   tracer concentration, which is also averaged vertically during day 9-20, is plotted in black

473   contours. The source regions of tracers are cross-hatched in the map. In addition, the simulated

474   July to August climatological wind, averaged from 800 to 200 hPa, is shown in Figure 6f, with

475   meridional wind in shadings and zonal wind in contours, both comparing well with the

476   observational reanalysis (not shown). Note that, as the goal here is to understand the transport

477   into the Arctic, we will focus on the meridional transport in the high latitudes (around 50°-70°N).

478   Details about tracer concentration and meridional flux in the mid-to-lower latitudes will not be

479   discussed. The amplitude of meridional flux depends on the concentration of the tracers during

480   day 9-20, while the concentration is determined by the amount of tracers released during day 1

481   and the amount of tracers removed throughout day 1-20. Since the amount of tracers that is

482   released and removed from different source regions can be different, we do not focus on

483   comparing the amplitude of concentration or meridional flux among different regions, but rather

484   focus on what the favorable locations are for tracers to be transported into the Arctic.

485   In Figure 6a-e, for tracers released in each source region, there are large tracer

486   concentrations located downstream (eastward) of the source regions in the mid-to-high latitudes,

487   consistent with zonal transport by the jet stream (Figure 6f) from days 9-20. The transport of

488   tracers is westward in the subtropics and tropics. The downstream (eastward) long-range zonal

489   transport of tracers from different emission regions (e.g. Asian, Europe and North America) has

490   been investigated in previous studies by using both observations and model simulations (e.g.

491   Akimoto 2003; Chin et al., 2007; Duncan and Bey 2004; Fang et al., 2009; Hudman et al., 2004;

492   Huntrieser et al., 2005; Lewis et al., 2007; Li et al., 2002; Liang et al., 2004). For ASI tracers

493   (Figure 6a), the large tracer concentration extends from eastern north Pacific to North Atlantic,

494   with strong northward flux into the Arctic located over Alaska and northern North Atlantic.

495   Large tracer concentration is found over central to eastern North Pacific for PAC tracers, and

496   part of the PAC tracers have also been transported into the northern North Atlantic (Figure 6b).

497   The northward flux of PAC tracers into the Arctic is also located over Alaska and North Atlantic.

498   Note that the distribution of meridional tracer transport (both northward and southward transport)

499   for ASI and PAC tracers (Figure 6a-b) matches well with the distribution of the climatological

500   meridional wind (Figure 6f). This suggests that Alaska and northern North Atlantic, where the

501   climatological meridional wind is northward, are the favorable locations for tracers to be

502   transported into the Arctic. Note that, the transport into the Arctic over these two regions (Alaska

503   and northern North Atlantic) is not necessarily via the climatological wind only, since these two

504   regions are also favorable for northward transport by transient eddies as they are located at the

505   exit region of the Pacific and Atlantic storm tracks. Additional analysis shows that northward

506   transport over the northern North Atlantic is dominated by contribution from climatological

507   wind, while both climatological wind and transients are important for northward transport of

508   PAC tracers over Alaska (Figure S1).

509   The distribution of the meridional flux for NAM, ATL and EUR tracers (Figure 6c-e),

510   also corresponds well with the distribution of the climatological meridional wind (Figure 6f)

511   except for a much weaker magnitude for ATL and EUR tracers compared to other tracers. For

512   ATL and EUR tracers, a large proportion of the tracers is transported downstream into Eurasia.

513   With climatological wind generally flowing southward over eastern Europe and western Siberia

514   (around 60°E) as well as over eastern Siberia (around 150°E), the net meridional transport of

515   tracers is southward for ATL and EUR tracers. Therefore, ATL and EUR tracers are not

516   effectively transported into the Arctic during day 9-20. In Figure 6c, the NAM tracer is also

517   transported into the North Atlantic where it is favorable for northward transport into the Arctic.

518   This zonal transport can happen in relatively short time compared to ASI tracers being

519   transported to the eastern North Pacific or PAC tracers to the North Atlantic, because of the

520   closer proximity between North America and North Atlantic. Thus, the intermediate transport

521   pathway can happen rather quickly for NAM tracers, which is the reason why the meridional flux

522   into the Arctic is positive during the first 10 days for NAM tracers (Figure 2c). However, when

523   the NAM tracers are transported further downstream into Europe, where the climatological flow

524   is generally southward, the net meridional flux of NAM tracers turns negative. This explains why

525   the NAM meridional tracer flux shifts to negative after 10 days (Figure 2c). The peak tracer

526   concentration at 10 days for NAM tracers (Figure 1e-f), which is in between the peak time of

527   ATL and EUR tracers (6-9 days), and ASI (10-30 days) and PAC tracers (10-15 days; see Figure

528   2), is due to the combination of the fast transport pathway and the intermediate transport

529   pathway. The fact that climatological northward flow is located over Alaska and North Atlantic,

530   rather than other regions around the Arctic, can be the main reason why both time-mean and

531   transient transports are important for PAC and ATL tracers for the fast transport pathway, while

532   transport by transients dominates for ASI, ATL and EUR tracers (Figure 5a, c and e; also see

533   section 4.2 for more details).

534   Note that TP and NI tracers also show a concentration peak at around 40-60 days in the

535   troposphere (Fig. 1e-f), but with little contribution to the total Arctic tracer concentration (Fig.

536   1b-c). Our analysis (not shown) suggests that the mechanism of this 40-60 day peak is similar to

537   the intermediate transport pathway for midlatitude tracers discussed above. The TP/NI tracers are

538   transported zonally by the jet first, and then can be transported into the Arctic over Alaska and

539   the northern North Atlantic. However, as the source regions of TP and NI tracers are over the

540   southern flank of the jet stream (Fig. 6f), it takes longer time for these tracers to be transported to

541   the northern flank of the jet where they can be transported into the Arctic. Whereas for

542   midlatitude source regions, the majority of the tracers are already at the northern flank of the jet

543   where they are released. Therefore, the intermediate transport pathway can happen much earlier

544   for the midlatitude tracers than for subtropical tracers (TP and NI).

545   In short, during day 9-20, the tracers are transported downstream (eastward) by the zonal

546   wind in the midlatitudes. ASI and PAC tracers are carried to Alaska and North Atlantic, and then

547   transported into the Arctic, as these two locations are favorable for northward transport into the

548   Arctic, leading to the intermediate transport timescales. However, as ATL and EUR tracers are

549   advected downstream to Eurasia, where it is favorable for southward transport, they are not

550   effectively transported into the Arctic during day 9-20, exhibiting no intermediate transport

551   pathway. Note that our results that Alaska and North Atlantic are the favorable locations for

552   northward transport into the Arctic, are in agreement with the model simulation results in

553   previous studies (e.g. Akimoto 2003, Hudman et al., 2004; Li et al., 2002; Liang et al., 2004).

554   The meridional transport pattern corresponds well with time-mean (decadal-mean) wind pattern,

555   suggesting that low frequency variability, which can lead to variability in the mean wind, can

556   likely lead to interannual or decadal variability of the intermediate transport pathway.

557   4.4 The Slow Transport Pathway

558   We now examine the transport of tracers from tropical and subtropical regions (NI, TP,

559   TR) into the Arctic lower stratosphere, with the peak tracer concentration occurring at around

25

560   100 days. We will discuss the transport of TP tracers in detail as TP tracers are most efficiently

561   transported into the Arctic among the three regions (Figure 1g). Later on, we will also show that

562   the mechanism for NI and TR tracers is very similar to that for TP tracers.

563   The zonal mean tendency of TP tracers, from day 1 to 100, is shown in Figure 7. During

564   the first few days after the tracers are released, the tendency of tracer concentration (Figure 7a-b,

565   shadings) indicates that tracers are brought up effectively into the subtropical UTLS region.

566   Subsequently, those tracers are transported both equatorward and poleward from the tracer

567   concentration maximum in the subtropics (black contours; Figure 7b-c). From days 11 to 100

568   (Figure 7d-h), a dipole pattern of the tracer tendency can be found in the UTLS in the tropics and

569   subtropics, with a positive tendency above the tracer concentration maximum, and a negative

570   tendency below, indicating a further upward lifting of the tracer concentration to about 80 hPa

571   during day 81-100.

572   The growth of tracer concentration above the Arctic for TP tracers (Figure 1g) starts

573   around days 20 to 30 after the tracers are released. The tendency of the tracers from day 21-100

574   shows a broad positive tendency over the midlatitude and polar lower stratosphere regions

575   (Figure 7e-h), with a larger tendency during day 21-60 (Figure 7e-f) than that during day 61-100

576   (Figure 7g-h; note the scale of Figure 7e-f and g-h is different). It can be seen that the positive

577   tendency over the midlatitude and polar regions can be traced back to the maximum tracer

578   concentration near 120-70 hPa in the tropics and subtropics approximately following the

579   isentropic surfaces (green contours). This suggests that the transport of tracers into the

580   midlatitude and polar regions is likely through isentropic transport from the tropics and

581   subtropics, when the large tracer concentration in the lower latitudes acts as a tracer reservoir.

582   So how are the tracers transported upward into the tropical and subtropical lower

583   stratosphere? We first show the time scale of the vertical transport (Figure 8a) by displaying the

584   time evolution of tracer concentration averaged over 0-40°N (also averaged zonally) at different

585   pressure levels. The peak time of the concentration increases as a function of the vertical levels

586   from about 5 days to 120 days for pressure levels from 125 hPa to 70 hPa. Thus, it takes on the

587   order of 100 days to vertically transport tracers within the tropical and subtropical lower

588   stratosphere.

589   The horizontal structure of the vertical transport in the lower latitudes is shown at 125,

590   100, 90 and 80 hPa (Figure 8b-c, f-g). We plot the vertical fluxes of tracers (red for upward, blue

591   for downward) averaged over 1-80 days, as the tracer concentration peaks at around 80 days for

592   80 hPa (Figure 8a). The vertical flux mostly happens from 10°E to 120°E in the subtropical

593   region, with upward flux in the east and downward flux in the west. In addition to the vertical

594   flux, the July to September modeled climatological vertical velocity is shown at the same

595   pressure levels (Figure 8d-e, h-i). Comparing the horizontal structure of vertical flux and vertical

596   velocity (Figure 8 b vs. d, c vs. e, f vs. h, g vs. i), they are rather consistent. The area averaged

597   (0°-40°N; 0-135°E) ascent, is about -5.1×10^{-4}Pa/s at 100 hPa and -2.7×10^{-4}Pa/s at 80

598   hPa. For an airmass to rise by 10 hPa, it takes about 23 days with the vertical velocity of

599   -5.1×10^{-4}Pa/s (at 100 hPa), and about 43 days with the vertical velocity of-2.7×10^{-4}Pa/s

600   (at 80 hPa). Consistent with Figure 8a, it takes about a month for TP tracers to rise by 10 hPa

601   above the 100 hPa level.

602   For TP tracers, the vertical transport in the UTLS region is mostly due to the dipole

603   structure of the vertical velocity from 10°E to 120°E, with upward motion in the east and

604   downward motion in the west, which coherently exists at all 4 levels in Figure 8. This dipole

605   structure of vertical motion, associated with the upper level anti-cyclone over the Asian summer

606   monsoon region, has been documented by previous studies (e.g., Bergman et al., 2013; Fu et al.,

607   2006; Orbe et al., 2015a; Pan et al., 2016; Park et al., 2009; Randel et al., 2010; Rodwell and

608   Hoskins 1996, 2001; Tissier & Legras, 2016; Vogel et al., 2015, 2019). The strong rising motion

609   directly above the source region of NI and TP tracers in the UTLS, is likely the reason why NI

610   and TP tracers can be most efficiently transported into lower latitude UTLS (Figure 7a; also see

611   Wu et al., 2020) and then into the Arctic (Figure 1g).

612   The transport pathway for NI and TR tracers is similar to TP tracers. The evolution of the

613   tracer tendency (Figure S2 for NI and Figure S3 for TR), is similar to TP (Figure 7) as we see

614   broad positive tendency over the midlatitude and polar lower stratosphere from day 21-100,

615   which is at the same potential temperature levels as the maximum tracer concentration in the

616   lower latitudes. Again, this implies isentropic transport from the tropics into high latitudes. The

617   vertical transport of tracers in the lower latitudes is shown in Figure S4 for NI and Figure S5 for

618   TR. Consistent with TP tracer, the vertical tracer fluxes follow the climatological vertical

619   velocity. Note that for TR tracers, upward transport in the lower stratosphere can happen both in

620   the tropics and in the subtropical summer monsoon regions. Thus, TR tracers are not only lifted

621   up locally, but also transported horizontally into regions favorable for upward transport and then

622   brought up by the vertical motion.

623

624   **5. Discussions and Conclusions**

625   In this study, we investigate the summertime transport pathways from different surface

626   regions in the NH into the Arctic by implementing and analyzing a large ensemble of idealized

627   tagged tracers in WACCM5. Three different transport pathways have been identified by

628   examining the temporal tracer concentration evolution in the Arctic. The fast transport pathway

629   can bring tracers from all midlatitude regions into the Arctic within the troposphere on time

630   scales less than 8 days. The intermediate transport pathway transports tracers released over Asia

631   and Pacific into the Arctic in 9-20 days. The slow transport pathway brings tropical and

632   subtropical tracers into the Arctic lower stratosphere in 1-3 months.

633   The fast transport pathway, which works efficiently for all the midlatitude regions, brings

634   tracers directly to the north from the source region into the Arctic in both the upper and lower

635   troposphere through meridional transport. The meridional and vertical processes relevant for the

636   fast transport pathway is summarized in the schematic diagrams (Figure 9a-b). During the first

637   two days after the tracers are released (Figure 9a), the tracers are lifted upward into the lower

638   troposphere by vertical diffusion. Furthermore, tracers are also transported into the upper

639   troposphere during the first two days by deep convection and transient vertical transport. Strong

640   poleward transport locates in the lower troposphere at around 60°N, which is at the northern

641   boundary of the source region. The northward transport in the upper troposphere is broader but

642   weaker compared to that in the lower troposphere. During day 3-8 (Figure 9b), as the tracer

643   concentration at the surface reduces due to surface deposition, vertical diffusion brings the

644   tracers downward back to the surface in the lower troposphere. However, vertical transport by

645   transients continues to bring tracers upward into the upper troposphere. The meridional transport

646   into the Arctic is dominated by transients for tracers released in Asia, Europe and North

647   America, while both time-mean and transient transports are important for tracers released in the

648   Pacific and the Atlantic. Note that Yang et al., (2019) used a different framework to decompose

649   the meridional transport of idealized tracers into zonal mean and zonally varying components,

650   and they found both zonal mean and zonally varying components can be important for poleward

651   transport. Here we focus on the time-mean component and deviations from the time mean. The

652   conclusions from different frameworks highlight the roles of different circulation features in

653   transporting tracers poleward.

654   The intermediate transport pathway transports the tracers into the Arctic on the time scale

655   of 1-3 weeks (Figure 9c). The tracers are first transported zonally by the jet stream. Then, if the

656   tracers are transported into regions that are favorable for northward transport into the Arctic,

657   which are over Alaska and the northern North Atlantic, then these tracers can be further

658   transported into the Arctic. For tracers released in Asia and the Pacific, as the source regions are

659   located upstream (west) of the favorable northward transport locations (Alaska and northern

660   North Atlantic), tracers can be advected by the zonal jet and then efficiently transported into the

661   Arctic via the intermediate transport pathway. However, for tracers released in Europe and the

662   Atlantic, as the source regions are located downstream (east) of the two favorable northward

663   transport locations, the zonal jet transports these tracers into locations (Eurasia) favorable for

664   southward transport out of the Arctic. Thus, Europe and Atlantic tracers do not exhibit a clear

665   intermediate transport pathway.

666   The fast and intermediate transport pathways have distinct features. The timescales of the

667   transport are different, and the ways the tracers are transported horizontally are also different.

668   The tracers are transported directly to the north via the fast transport pathway while they are first

669   advected zonally before transported northward into the Arctic via the intermediate transport

670   pathway. These are new findings that have not been documented by previous studies. In addition,

671   we utilize a detailed budget analysis of tracer concentration as well as a decomposition analysis

672   of the transport into time mean and transient components to understand the mechanism of the

673   two pathways. This is also a novel aspect of this study.

674   The slow transport pathway carries the tropical and subtropical tracers into the Arctic

675   lower stratosphere. A schematic diagram for the slow transport pathway is shown in Figure 9d.

676   The tracers are first effectively brought up into the upper troposphere in the tropics and

677   subtropics, mostly by deep convection and large-scale ascent. Then, the tracers are slowly

678   transported upward into the lower stratosphere at locations where the climatological upward

679   motion is prominent. These locations for upward transport into the lower stratosphere are not

680   limited to the tropics, as strong vertical motion can also be found in the UTLS in the summer

681   monsoon regions. The transport pathway into the UTLS in the summer monsoon regions has

682   been well documented by previous studies (e.g. Pan et al., 2016; Park et al., 2009; Randel et al.,

683   2010 and others). The results from a few previous studies (e.g. Bourassa et al., 2012; Orbe et al.,

684   2015) suggest that tracer species or aerosols can be transported to the Arctic after they are lifted

685   up into the lower stratosphere over the summer monsoon region. Our study shows more details

686   about this transport pathway and associated timescales. The tracers are first lifted up from100

687   hPa to 70 hPa over the monsoon region on one to four months' time scale, and they can then be

688   transported into the midlatitude and the Arctic following the isentropes. As the climatological

689   upward motion during summer is the strongest over the Asian monsoon region, tracers released

690   in northern India and Tibetan Plateau, which are right beneath the upper level rising motion, can

691   be most efficiently transported into the Arctic via the slow transport pathway.

692   In this study, we focus on understanding the main features of the three different transport

693   pathways. These transport pathways can have month-to-month (e.g. July vs August), interannual

694   and decadal variabilities as the circulation pattern changes. Our preliminary analysis suggests

695   that, as the circulation structure is not very different between July and August, the time scale and

696   circulation processes involved in these pathways are similar, whereas the spatial pattern of the

697   meridional transport for fast and intermediate can be slightly different (not shown). The slow

698   transport pathway is slightly more efficient during July than August, which is likely because

699   tracers are more efficiently transported into the UTLS over the Asian summer monsoon region

700   during July as pointed out by Wu et al., (2020). The time-mean wind pattern can also be different

701   during different years or decades due to low frequency variability, suggesting that there could be

702   substantial interannual or decadal variability for fast and intermediate transport pathways. The

703   variability of Asian summer monsoon can also lead to interannual variability of the slow

704   transport pathway. These topics are currently being explored and will be reported in future

705   studies.

706   Consistent with Orbe et al., (2015a), our results indicate that midlatitude source regions

707   contribute the most to the passive tracer concentration within the Arctic troposphere, whereas

708   tropical and subtropical source regions contribute the most in the Arctic lower stratosphere. Our

709   findings also suggest that pollutants emitted over all NH midlatitude land regions could be

710   quickly transported into the Arctic troposphere within about one week via the fast transport

711   pathway. Tracer species and aerosols emitted over Asia and North America could also be

712   transported into the Arctic troposphere in about one to three weeks via the intermediate transport

713   pathway. Regions like northern India and Tibetan Plateau are highlighted by the slow transport

714   pathway and might have important implications for the transport of chemical species, such as

715   ozone depleting substances, to the Arctic lower stratosphere. The approach with idealized tracers

716   that have a spatially uniform source in this study focuses on the role of atmospheric dynamics

717   underlying the transport pathways. To properly attribute the Arctic concentration of different

718   chemical species to different source regions, the spatial distribution of emission (e.g.

719   anthropogenic emission) needs to be taken into account. Future work will be devoted to linking

720   the idealized tracer results to realistic emission sources and their implications.

721

References

Atlas, E. L., B. A. Ridley, and C. A. Cantrell, 2003: The Tropospheric Ozone Production about the Spring Equinox (TOPSE) Experiment: Introduction. J. Geophys. Res., 108, 8353, doi:10.1029/2002JD003172.

Akimoto, H. (2003), Global air quality and pollution, Science, 302, 1716– 1719, doi:10.1126/science.1092666.

Bergman, J. W., Fierli, F., Jensen, E. J., Honomichl, S., & Pan, L. L. (2013). Boundary layer sources for the Asian anticyclone: Regional contributions to a vertical conduit. Journal of Geophysical Research: Atmospheres, 118, 2560–2575. https://doi.org/10.1002/jgrd.50142

Bottenheim, J. W., Dastoor, A., Gong, S. L., Higuchi, K., and Li, Y. F. 2004: Long Range Transport of Air Pollution to the Arc- tic, in: Handbook of Environmental Chemistry, vol. 4G, 13–39, Springer, Berlin, Heidelberg, https://doi.org/10.1007/b94522.

Bond, T. C., Doherty, S. J., Fahey, D. W., Forster, P. M., Berntsen, T., DeAngelo, B. J., Flanner, M. G., Ghan, S., Kärcher, B., Koch, D., Kinne, S., Kondo, Y., Quinn, P. K., Sarofim, M. C., Schultz, M. G., Schulz, M., Venkataraman, C., Zhang, H., Zhang, S., Bellouin, N., Guttikunda, S. K., Hopke, P. K., Jacob- son, M. Z., Kaiser, J. W., Klimont, Z., Lohmann, U., Schwarz, J. P., Shindell, D., Storelvmo, T., Warren, S. G., and Zender, C. S.: Bounding the role of black carbon in the climate sys- tem: A scientific assessment, J. Geophys. Res., 118, 5380–5552, doi:10.1002/jgrd.50171, 2013

Bourassa, A. E., A. Robock, W. J. Randel, T. Deshler, L. A. Rieger, N. D. Lloyd, E. J. Llewellyn, and D. A. Degenstein (2012), Large volcanic aerosol load in the stratosphere linked to asian monsoon transport, Science, 337(6090), 78– 81, doi:10.1126/science.1219371.

758   Chin, M., R. B. Rood, S.-J. Lin, J.-F. Müller, and A. M. Thompson (2000), Atmospheric sulfur

759   cycle simulated in the global model GOCART: Model description and global properties,

760   J. Geophys. Res., 105, 24,671– 24,687, doi:10.1029/2000JD900384.

761   Coopman, Q., Garrett, T. J., Finch, D. P., and Riedi, J.(2018): High Sensitivity of Arctic Liquid

762   Clouds to Long-Range Anthro- pogenic Aerosol Transport, Geophys. Res. Lett., 45, 372–

763   381, https://doi.org/10.1002/2017GL075795.

764   Duncan, B. N., and I. Bey (2004), A modeling study of the export pathways of pollution from

765   Europe: Seasonal and interannual variations (1987–1997), J. Geophys. Res., 109,

766   D08301, doi:10.1029/2003JD004079.

767   Fang, Y., A. M. Fiore, L. W. Horowitz, A. Gnanadesikan, H. Levy, Y. Hu, and A. G. Russell

768   (2009), Estimating the contribution of strong daily export events to total pollutant export

769   from the United States in summer, J. Geophys. Res., 114, D23302,

770   doi:10.1029/2008JD010946.

771   Fisher, J. A., Jacob, D. J., Purdy, M. T., Kopacz, M., Le Sager, P., Carouge, C., Holmes, C. D.,

772   Yantosca, R. M., Batchelor, R. L., Strong, K., Diskin, G. S., Fuelberg, H. E., Holloway, J.

773   S., Hyer, E. J., McMillan, W. W., Warner, J., Streets, D. G., Zhang, Q., Wang, Y., and

774   Wu, S. 2010: Source attribution and interannual variability of Arctic pollution in spring

775   constrained by aircraft (ARCTAS, ARCPAC) and satellite (AIRS) observations of carbon

776   monoxide, Atmos. Chem. Phys., 10, 977–996, https://doi.org/10.5194/acp-10-977-2010.

777   Fu, R., Hu, Y., Wright, J. S., Jiang, J. H., Dickinson, R. E., Chen, M., et al. (2006). Short circuit

778   of water vapor and polluted air to the global stratosphere by convective transport over the

779   Tibetan Plateau. Proceedings of the National Academy of Sciences of the United States

780   of America, 103(15), 5664–5669. https://doi.org/10.1073/pnas.0601584103

781 Garcia, R. R., & Richter, J. H. (2019). On the momentum budget of the Quasi-Biennial

782   Oscillation in the Whole Atmosphere Community Climate Model. Journal ofthe

783   Atmospheric Sciences, 76, 69–87. https://doi.org/10.1175/JASD-18-0088.1

784 Garrett, T. J., and C. Zhao, 2006: Increased Arctic cloud longwave emissivity associated with

785   pollution from mid-latitudes. Nature, 440, 787–789, doi:10.1038/nature04636.

786 Haine, T. W. N., H. Zhang, D. W. Waugh, and M. Holzer. "On transit-time distributions in

787   unsteady circulation models." Ocean Modelling 21, no. 1-2 (2008): 35-45.

788 Hansen, J., and L. Nazarenko, 2004: Soot climate forcing via snow and ice albedos. *Proceedings*

789   *of the National Academy of Sciences of the United States of America*, 101, 423–428,

790   doi:10.1073/pnas.2237157100.

791 Holzer, M., & Hall, T. M. (2000). Transit-time and tracer-age distributions in geophysical flows.

792   Journal of the AtmosphericSciences, 57, 3539–3558.

793 Holzer, M., I. G. McKendry, and D. A. Jaffe (2003), Springtime trans-Pacific atmospheric

794   transport from east Asia: A transit-time probability density function approach, J. Geophy

795   s. Res., 108(D22), 47 08,doi:10.1029/2003JD003558

796 Hudman, R. C., et al. (2004), Ozone production in transpacific Asian pollution plumes and

797   implications for ozone air quality in California, J. Geophys. Res., 109, D23S10,

798   doi:10.1029/2004JD004974.

799 Huntrieser, H., et al. (2005), Intercontinental air pollution transport from North America to

800   Europe: Experimental evidence from airborne measurements and surface observations, J.

801   Geophys. Res., 110, D01305, doi:10.1029/2004JD005045.

802 Hurrell, J. W., Holland, M. M., Gent, P. R., Ghan, S., Kay, J. E., Kushner, P. J., et al. (2013).

803   The Community Earth System Model: A framework for collaborative research. Bulletin

804   of the American Meteorological Society, 94, 1339–1360. https://doi.org/10.1175/ BAMS-

805   D-12-00121.1

806 Ikeda, K., Tanimoto, H., Sugita, T., Akiyoshi, H., Kanaya, Y., Zhu, C., & Taketani, F. (2017).

807   Tagged tracer simulations of black carbon in the arctic: Transport, source contributions,

808   and budget. Atmospheric Chemistry and Physics, 17(17), 10,515– 10,533.

809 Krishnamurti, T. N., R. Krishnamurti, S. Das, V. Kumar, A. Jayakumar, and A. Simon, 2015: A

810   pathway connecting the monsoonal heating to the rapid Arctic ice melt. J. Atmos. Sci.,

811   72, 5–34, https://doi.org/10.1175/JAS–D–14–0004.1.

812 Klonecki, A., P. Hess, L. Emmons, L. Smith, J. Orlando, and D. Blake, 2003: Seasonal changes

813   in the transport of pollutants into the Arctic troposphere-model study. J. Geophys. Res.,

814   108, 8367, doi:10.1029/2002JD002199.

815 Koch, D., and J. Hansen (2005), Distant origins of Arctic black carbon: AGoddard Institute for

816   Space Studies ModelE experiment, J. Geo phys.Res., 110, D04204,

817   doi:10.1029/2004JD005296

818 Kupiszewski, P., Leck, C., Tjernström, M., Sjogren, S., Sedlar, J., Graus, M., Müller, M.,

819   Brooks, B., Swietlicki, E., Norris, S., and Hansel, A. 2013: Vertical profiling of aerosol

820   particles and trace gases over the central Arctic Ocean during summer, Atmos. Chem.

821   Phys., 13, 12405–12431, https://doi.org/10.5194/acp-13-12405-2013.

822 Laliberte, F. and P. J. Kushner, 2014: Midlatitude moisture contribution to recent Arctic

823   tropospheric summertime variability. J. Climate, 27, 5693–5707,

824   https://doi.org/10.1175/JCLI–D–13–00 721.1.

825 Law, K. S., and A. Stohl, 2007: Arctic air pollution: Origins and impacts. Science, 315, 1537–

826   1540, doi:10.1126/science.1137695.

827   Li, Q., et al. (2002), Transatlantic transport of pollution and its effects on surface ozone in

828   Europe and North America, J. Geophys. Res., 107(D13), 4166,

829   doi:10.1029/2001JD001422.

830   Li, F., Waugh, D. W., Douglass, A. R., Newman, P. A., Pawson, S., Stolarski, R. S., et al.

831   (2012). Seasonal variations of stratospheric age spectra in the Goddard Earth Observing

832   System Chemistry Climate Model (GEOSCCM). Journal ofGeophysical Research, 117,

833   D05134. https://doi.org/10.1029/2011JD016877

834   Liang, Q., L. Jaeglé, D. A. Jaffe, P. Weiss-Penzias, A. Heckman, and J. A. Snow (2004), Long-

835   range transport of Asian pollution to the northeast Pacific: Seasonal variations and

836   transport pathways of carbon monoxide, J. Geophys. Res., 109, D23S07,

837   doi:10.1029/2003JD004402.

838   Liu, D., B. Quennehen, E. Darbyshire, J. D. Allan, P. I. Williams, J. W. Taylor, S. J.-B.

839   Bauguitte, M. J. Flynn, D. Lowe, M. W. Gallagher, K. N. Bower, T. W. Choularton, and

840   H. Coe, 2015: The importance of Asia as a source of black carbon to the European Arctic

841   during springtime 2013. Atmos. Chem. Phys., 15, 11 537–11 555,

842   https://doi.org/10.5194/acp–15–11 537–2015.

843   Liu, H., D. J. Jacob, I. Bey, R. M. Yantosca, B. N. Duncan, and G. W. Sachse, 2003: Transport

844   pathways for Asian pollution outflow over the Pacific: Interannual and seasonal

845   variations. J. Geophys. Res., 108(D20), 8786, doi:10.1029/2002JD003 102.

846   Lewis, A., et al. (2007), Chemical composition observed over the mid-Atlantic and the detection

847   of pollution signatures far from source regions, J. Geophys. Res., 112, D10S39,

848   doi:10.1029/2006JD007584.

849   Lubin, D., and A. M. Vogelmann, 2006: A climatologically significant aerosol longwave indirect

850   effect in the Arctic. Nature, 439, 453–456, doi:10.1038/nature04449.

851 Neale, R. B., Chen, C.-C., Gettelman, A., Lauritzen, P. H., Park, S., Williamson, D. L., et al.

852   (2010). Description of the NCAR Community Atmosphere Model (CAM 5.0). NCAR

853   Tech. Note NCAR/TN–486+STR, 282 pp

854 Orbe, C., Holzer, M., & Polvani, L. M. (2012). Flux distributions as robust diagnostics of

855   stratosphere-troposphere exchange. Journal of Geophysical Research, 117, D01302.

856   https://doi.org/10.1029/2011JD016455

857 Orbe, C., P. A. Newman, D. W. Waugh, M. Holzer, L. D. Oman, F. Li, and L. M. Polvani,

858   (2015a): Airmass origin in the Arctic. Part I: Seasonality. J. Climate, 28, 4997–5014,

859   doi:10.1175/ JCLI-D-14-00720.1.

860 Orbe, Clara, Darryn W. Waugh, and Paul A. Newman. (2015b): Air-mass origin in the tropical

861   lower stratosphere: The influence of Asian boundary layer air." Geophysical Research

862   Letters 42, no. 10: 4240-4248.

863 Orbe, C., Waugh, D. W., Newman, P. A., & Steenrod, S. (2016). The transit-time distribution

864   from the Northern Hemisphere midlatitude sur-face. Journal of the Atmospheric

865   Sciences, 73, 3785–3802.

866 Pan, L. L., Honomichl, S. B., Kinnison, D. E., Abalos, M., Randel, W. J., Bergman, J. W., &

867   Bian, J. (2016). Transport of chemical tracers from the boundary layer to stratosphere

868   associated with the dynamics of the Asian summer monsoon. Journal of Geophysical

869   Research: Atmospheres, 121, 14,159–14,174. https://doi.org/10.1002/2016JD025616

870 Park, M., Randel, W. J., Emmons, L., & Livesey, N. (2009). Transport pathways of carbon

871   monoxide in the Asian summer monsoon diagnosed from from Model of Ozone and

872   Related Tracers (MOZART). Journal of Geophysical Research, 114, D08303.

873   https://doi.org/10.1029/2008JD010621

874   Park, S., & Bretherton, C. S. (2009). The University ofWashington shallow convection and moist

875   turbulence schemes and their impact on climate simulations with the Community

876   Atmosphere Model. Journal Climate, 22, 3449–3469.

877   https://doi.org/10.1175/2008JCLI2557.1

878   Ploeger, F., & Birner, T. (2016). Seasonal and inter-annual variability of lower stratospheric age

879   of air spectra. Atmospheric Chemistry and Physics, 16, 10195.

880   https://doi.org/10.5194/acp-16-10195-2016

881   Quinn P. K., G. Shaw, E. Andrews, E. G. Dutton, T. Ruoho-Airola & S. L. Gong (2007): Arctic

882   haze: current trends and knowledge gaps, *Tellus B: Chemical and Physical Meteorology*,

883   59:1, 99-114, DOI: 10.1111/j.1600-0889.2006.00236.x

884   Rahn, K. A., and R. J. McCaffrey, 1980: On the origin and transport of the winter Arctic aerosol.

885   Ann. N. Y. Acad. Sci., 338, 486– 503, doi:10.1111/j.1749-6632.1980.tb17142.x.

886   Randel, W. J., Park, M., Emmons, L., Kinnison, D., Bernath, P., Walker, K., et al. (2010). Asian

887   monsoon transport of pollution to the stratosphere. Science, 328, 611.

888   https://doi.org/10.1126/science.1182274

889   Rodwell, M. J., and B. J. Hoskins, 2001: Subtropical Anticyclones and Summer Monsoons. J.

890   Climate, 14, 3192–3211, https://doi.org/10.1175/1520-

891   0442(2001)014<3192:SAASM>2.0.CO;2.

892   Rodwell, M. J., and B. J.Hoskins, 2001: Subtropical anticyclones and summer monsoons.J.

893   Climate, 14, 3192–3211. https://doi.org/10.1002/qj.49712253408

894   Shindell, D. 2007: Local and remote contributions to Arctic warming, Geophys. Res. Lett., 34,

895   1–5, https://doi.org/10.1029/2007GL030221.

896   Shindell, D., and Coauthors, 2008: A multi-model assessment of pollution transport to the Arctic.

897   Atmos. Chem. Phys., 8, 5353– 5372, doi:10.5194/acp-8-5353-2008.

898   Stohl, A., 2006: Characteristics of atmospheric transport into the Arctic troposphere. J. Geophys.

899   Res., 111, D11306, doi:10.1029/ 2005JD006888.

900   Tissier, A.-S., & Legras, B. (2016). Convective sources of trajectories traversing the tropical

901   tropopause layer. Atmospheric Chemistry and Physics, 16, 3383–3398.

902   https://doi.org/10.5194/acp-16-3383-2016

903   Vogel, B., Günther, G., Müller, R., Grooß, J.-U., & Riese, M. (2015). Impact of different Asian

904   source regions on the composition of the Asian monsoon anticyclone and of the

905   extratropical lowermost stratosphere. Atmospheric Chemistry and Physics, 15, 13,699–

906   13,716. https://doi.org/10.5194/acp-15-13699-2015

907   Vogel, B., R., M., Günther, G., Spang, R., Hanumanthu, S., Li, D., et al. (2019). Lagrangian

908   simulations of the transport of young air masses to the top of the Asian monsoon

909   anticyclone and into the tropical pipe. Atmospheric Chemistry and Physics, 19, 6007–

910   6034. https://doi.org/10.5194/acp-19-6007-2019

911   Wang, X., Wu, Y., Tung, W.-W., Richter, J. H., Glanville, A. A., Tilmes, S., et al. (2018). The

912   simulation of stratospheric water vapor over the Asian summer monsoon region in

913   CESM1(WACCM) models. Journal ofGeophysical Research: Atmospheres, 123, 11,377–

914   11,391. https:// doi.org/10.1029/2018JD028971

915   Warren, S.G. and W.J. Wiscombe, 1980: A Model for the Spectral Albedo of Snow. II: Snow

916   Containing Atmospheric Aerosols. *Journal of the Atmospheric Sciences*, 37, 2734–2745,

917   https://doi.org/10.1175/1520-0469(1980)037<2734:AMFTSA>2.0.CO;2

918   Wu,Y., Orbe,C., Tilmes,S., Abalos, M., & Wang, X. (2020). Fast transport pathways into the

919   Northern Hemisphere upper troposphere and lower stratosphere during northern summer.

920   Journal ofGeophysical Research: Atmospheres, 125, e2019JD031552. https://doi.org/10.

921   1029/2019JD031552

922   Xu, J.-W., R. V. Martin, A. Morrow, S. Sharma, L. Huang, W. R. Leaitch, J. Burkart, H. Schulz,

923   M. Zanatta, M. D. Willis, D. K. Henze, C. J. Lee, A. B. Herber, and J. P. D. Abbatt,

924   2017: Source attribution of Arctic black carbon constrained by aircraft and surface

925   measurements. Atmos. Chem. Phys., 17, 11 971–11 989, https://doi.org/10.5194/acp–17–

926   11 971–2017.

927   Yang, H., Waugh, D. W., Orbe, C., Zeng, G., Morgenstern, O., Kinnison, D. E., & Schofield, R.

928   (2019). Large-scale transport into the Arctic: The roles of the midlatitude jet and the

929   Hadley Cell. Atmospheric Chemistry and Physics. https://doi.org/10.5194/acp-2018-841

930   Zhang, G. J., & McFarlane, N. A. (1995). Sensitivity of climate simulations to the

931   parameterization of cumulus convection in the Canadian Climate Centre general

932   circulation model. Atmosphere-Ocean, 33, 407–446.

933
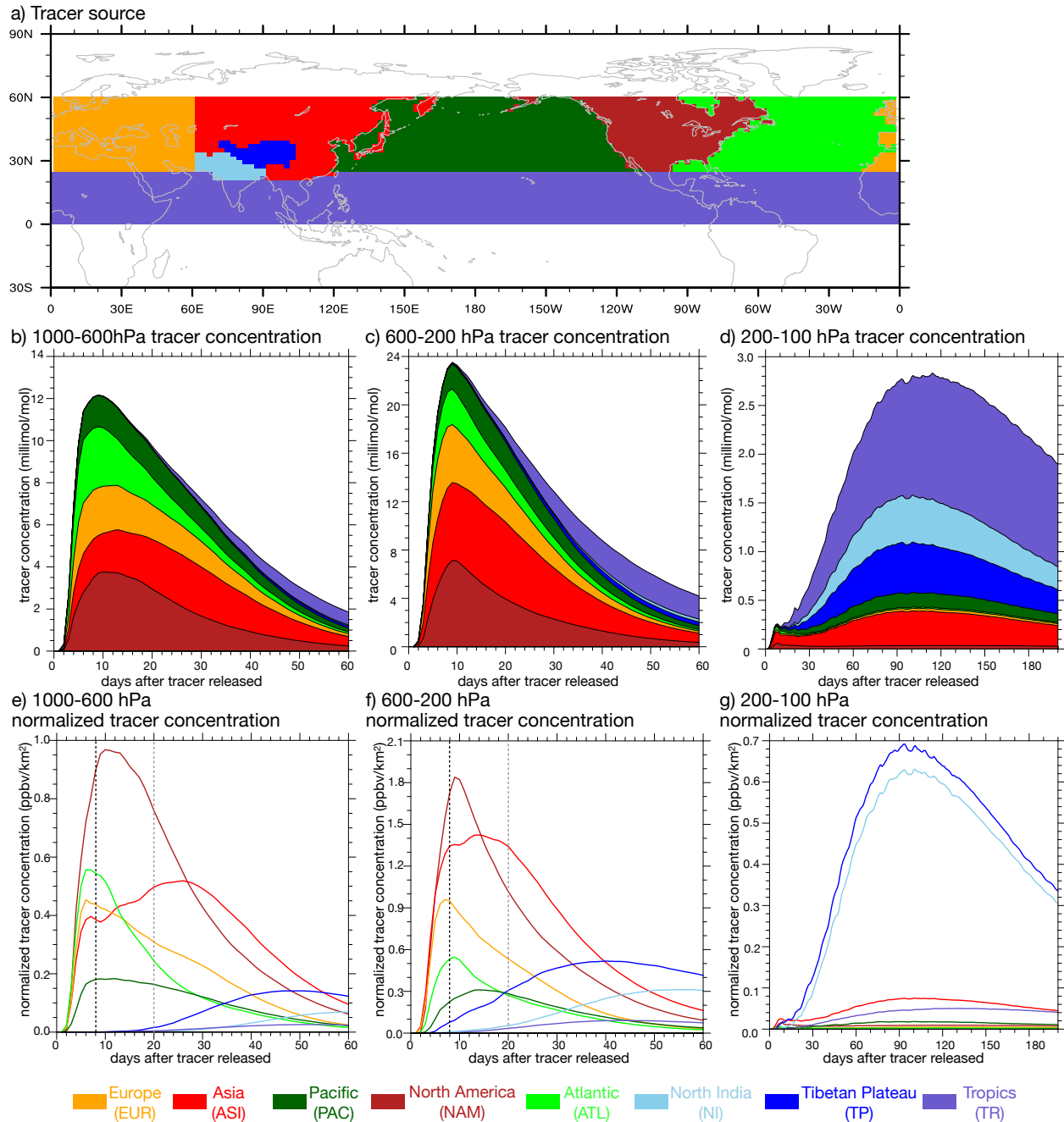
Figure 1. a) Definition of the source regions for EUR, ASI, PAC, NAM, ATL, NI, TP and TR tracers. b)-d) Temporal evolution of tracer concentration in the Arctic (north of 70°N) at 1000-600 hPa, 600-200 hPa and 200-100 hPa respectively. Each color shading represents tracers that are released in one region. Tracer concentration is multiplied by 1000. Unit in millimole/mole. e)-f) Temporal evolution of normalized tracer concentration in the Arctic at the same pressure levels in b)-d). Unit in ppbv/km². The tracer concentration is divided by the area of the source region as the tracer concentration is normalized (also see main text). The dashed black lines and dashed grey lines denote day 8 and day 20 after the tracers are released respectively in e)-f).

944
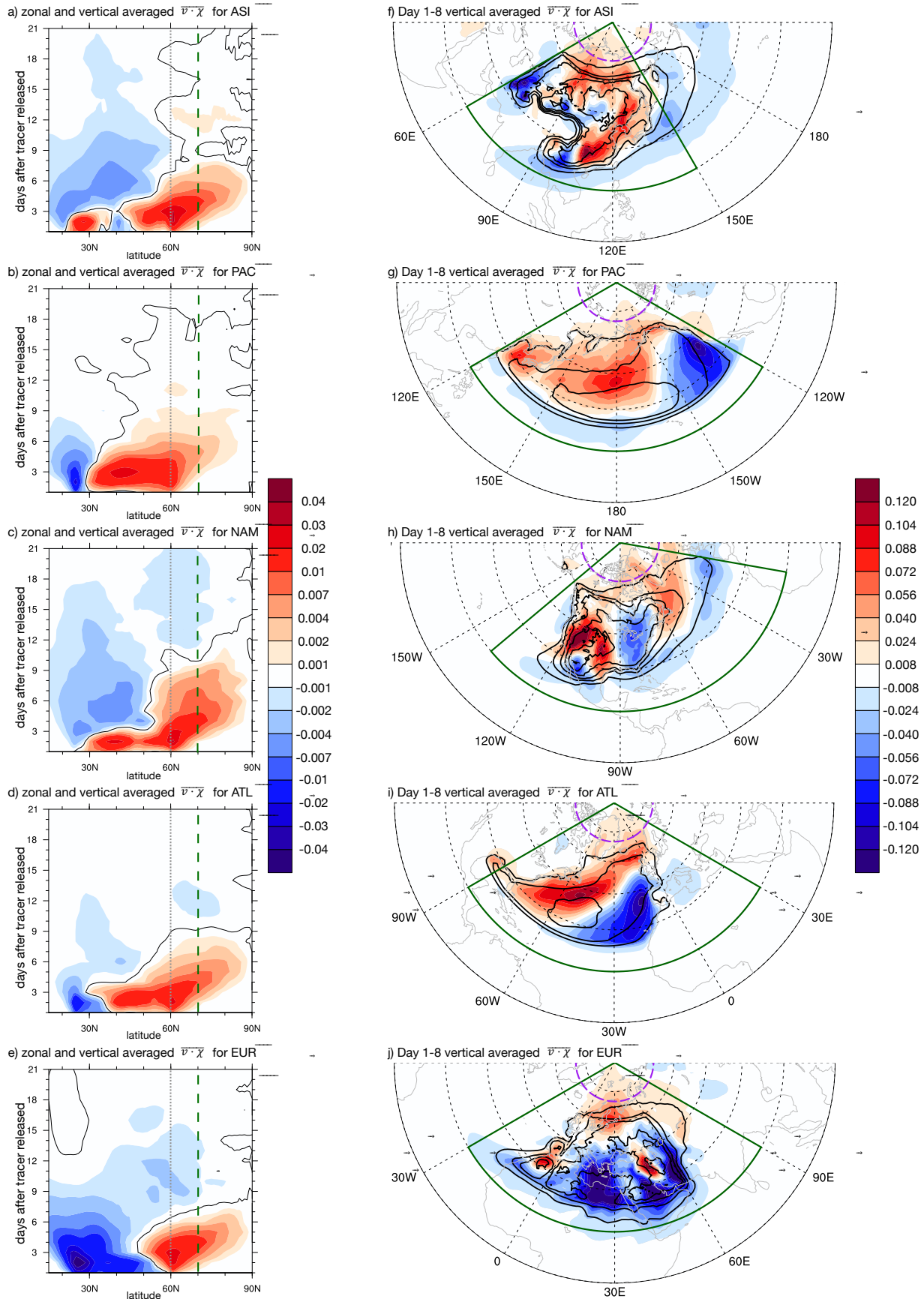
945   **Figure 2.** a) Zonally and vertically (1000-100 hPa) averaged tracer meridional flux at different
946   latitude (15°N-90°N) and different time (1-21 days) after the ASI tracers are released. The black
947   contour denotes the zero line and the dashed dark green line marks the boundary of the Arctic
948   region (70°N). The dashed gray line denotes the northern boundary of the tracer source region.
949   Unit of the meridional flux is in (mol/mol) · (m/s). b)-e) The same as a), but for PAC, NAM,
950   ATL and EUR tracers respectively. f) The shadings are vertically averaged (1000-100 hPa) tracer
951   meridional flux during day 1-8 for the ATL tracers. Unit in (mol/mol) · (m/s). Black contour
952   lines show the vertically averaged (1000-100 hPa) ASI tracer concentration during day 1-8. The
953   contour interval is 0.01 mol/mol. Dashed purple line denotes the boundary of the Arctic region
954   (70°N). g)-j) The same as f), but for PAC, NAM, ATL and EUR tracers respectively. In f)-j), the
955   regions defined by the dark green line are where further analysis will be performed in Figure 3-5.
956   The southern boundaries are at 15°N while the northern boundaries are at 90°N. The east and
957   west boundaries are 60°E-150°E in f), 120°E-120°W in g), 140°W-10°W in h), 90°W-30°E in i)
958   and 30°W-90°E in j).
959
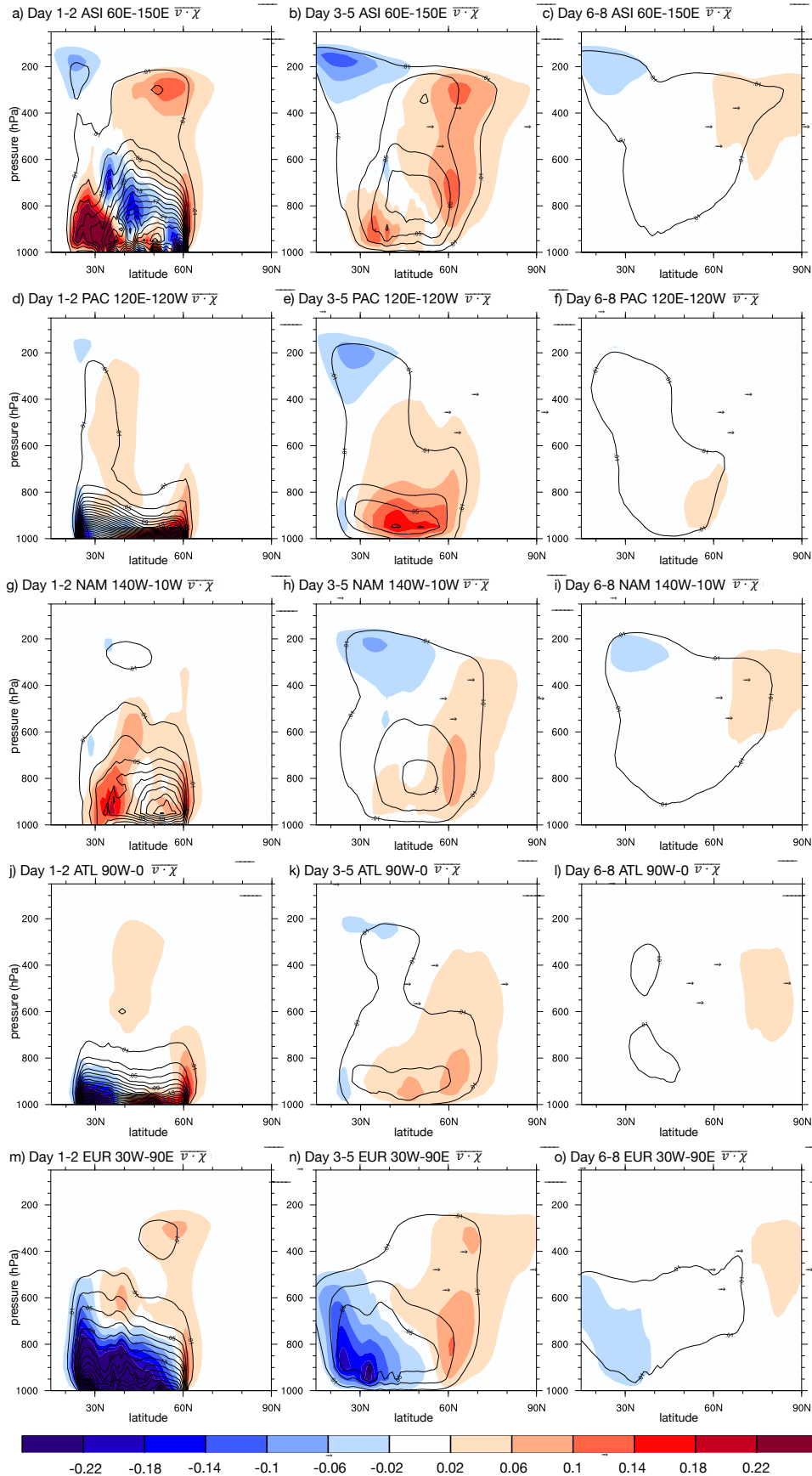
961 **Figure 3.** a) Meridional and vertical structure of tracer meridional flux and concentration during
962 day 1-2 for ASI tracers. The shadings are meridional flux of ASI tracers averaged over 60°E-
963 150°E (the region denoted by dark green line in Figure 2f). Unit in (mol/mol) · (m/s). The
964 contours are tracer concentration averaged also over 60°E-150°E. The contour lines start from
965 0.01 mol/mol, with an interval of 0.02 mol/mol. b)-c) The same as a), but for day 3-5 and 6-8. d)-
966 f) The same as a)-c) but for PAC tracers. The averaging is performed over 120°E-120°W (also
967 see Figure 2g). g)-i) The same as a)-c) but for NAM tracers. The averaging is performed over
968 140°W-10°W (also see Figure 2h). j)-l) The same as a)-c) but for ATL tracers. The averaging is
969 performed over 90°W-30°E (also see Figure 2i). m)-o) The same as a)-c) but for EUR tracers.
970 The averaging is performed over 30°W-90°E (also see Figure 2j).
971
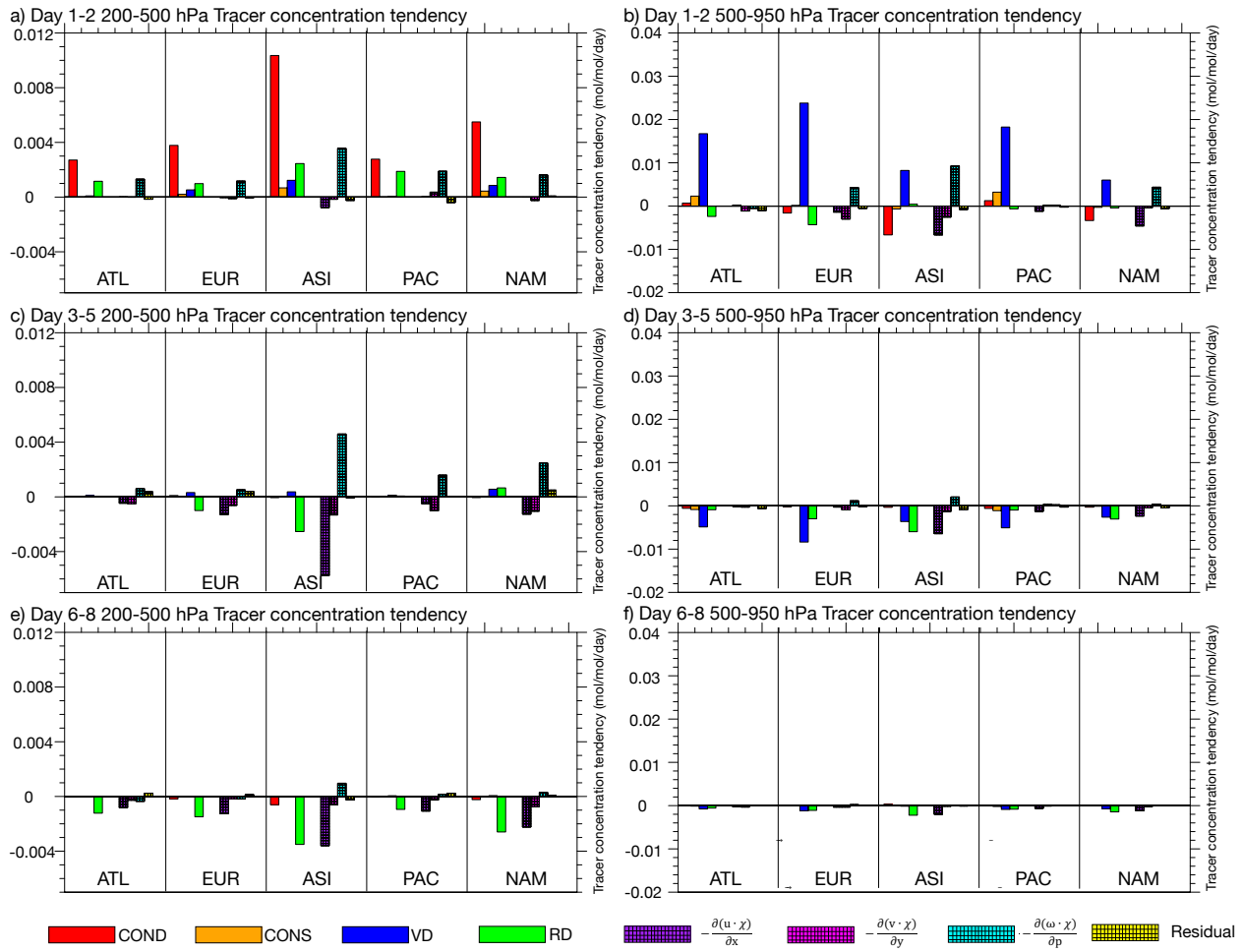
Figure 4. a) Tracer budget analysis during day 1-2 in the upper troposphere (200-500 hPa). Following equation (1), tracer tendency is separated into contribution from deep convection (red, COND), shallow convection (orange, CONS), vertical diffusion (blue, VD) and transport by resolved dynamics (green, RD). From equation (4), transport by resolved dynamics is further decomposed into zonal transport (crosshatched purple), meridional transport (crosshatched magenta) and vertical transport (crosshatched cyan). The residual of equation (4) due to using daily mean data to estimate the rhs of the equation, is in yellow shadings (crosshatched). The budget analysis for different tracers is performed over 30°N-70°N with the same east-west boundary in Figure 3. Unit is (mol/mol)/day. b) The same as a), but for 500-950 hPa. c)-d) The same as a)-b), but for day 3-5. e)-f) The same as a)-b), but for day 6-8.
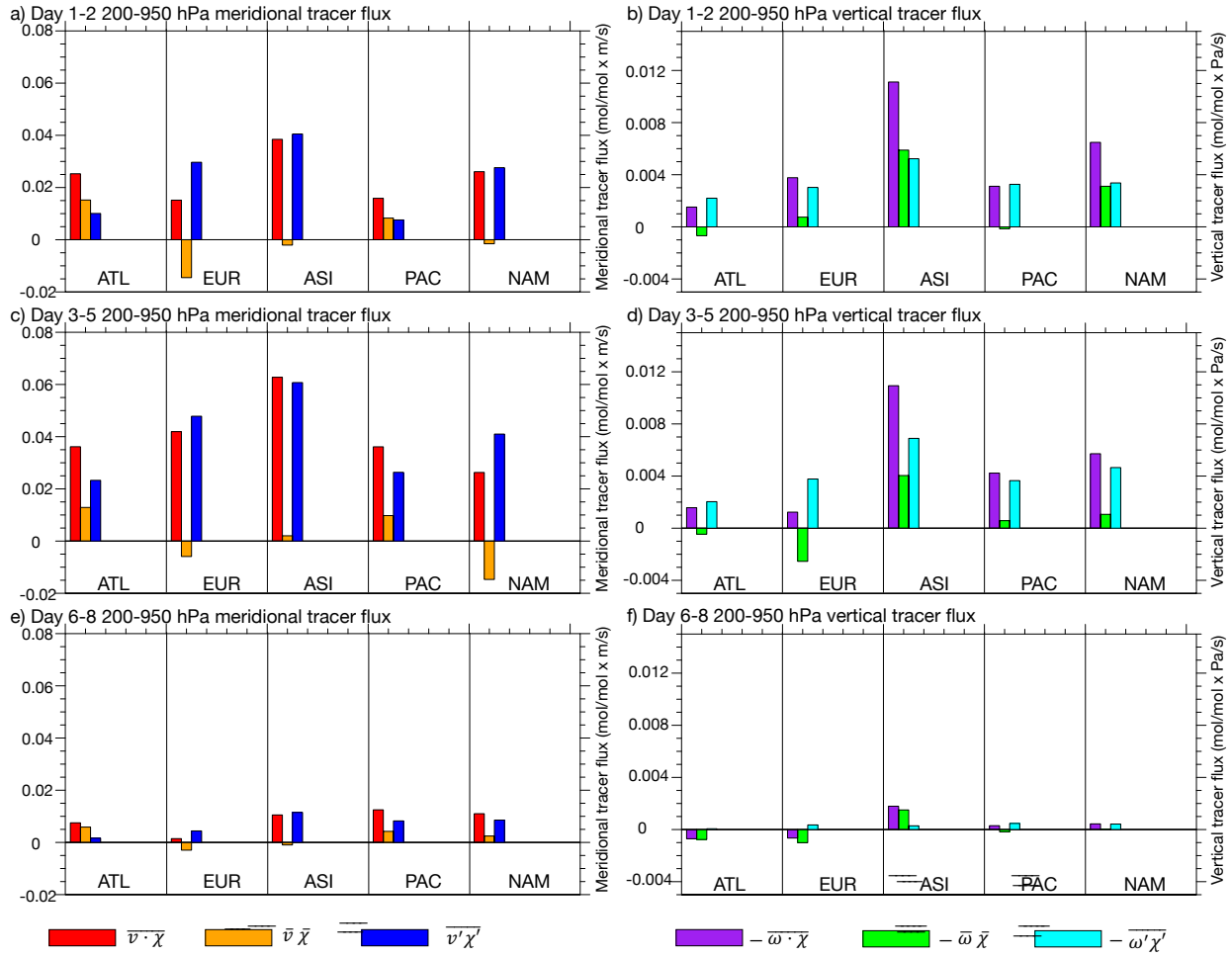
Figure 5. a) Decomposition of meridional tracer flux of different tracers during day 1-2 from 200-950 hPa. The decomposition of different tracers is performed over 50°N-70°N with the same east-west boundary in Figure 3. The total meridional flux is denoted by red, while the flux by climatological wind and transients is denoted by orange and blue respectively. Unit in (mol/mol) · (m/s). b) Similar to a), but for the decomposition of vertical tracer flux by resolved dynamics over 30°N-70°N with the same east-west boundary in Figure 3. The total upward flux is denoted by purple, while the flux by climatological wind and transients is denoted by green and cyan respectively. Unit in (mol/mol) · (m/s). c)-d) The same as a)-b), but for day 3-5. e)-f) The same as a)-b) but for day 6-8.

995
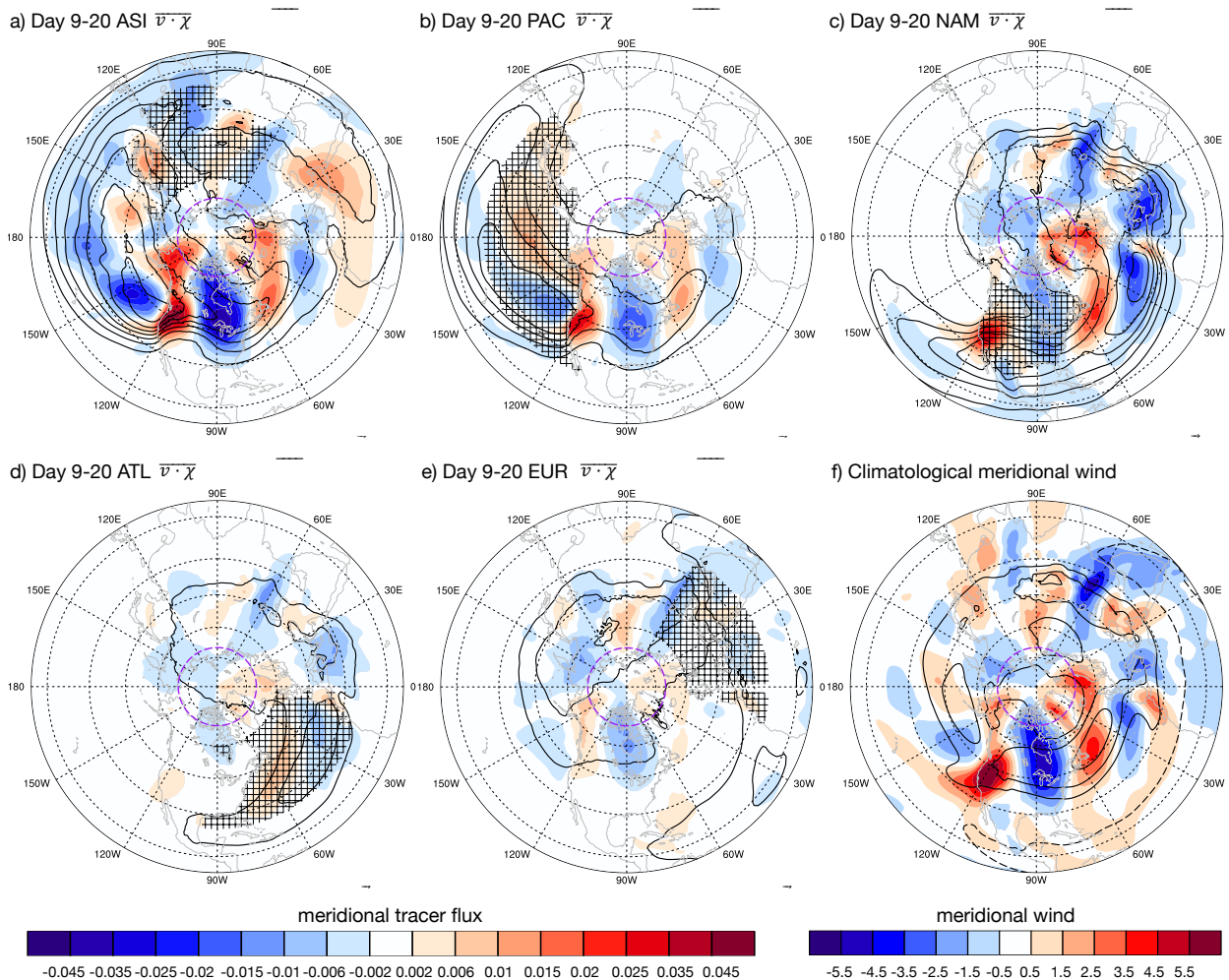
Figure 6. a) The shadings are the meridional tracer flux averaged vertically (1000-100 hPa) during day 9-20 for ASI tracers. Unit in $(mol/mol) \cdot (m/s)$. The black contours are the vertically averaged (1000-100 hPa) tracer concentration. Contour interval is 0.0015 mol/mol. The boundary of Arctic region is denoted by the dashed purple line. The source region of the tracers is crosshatched. b)-e) The same as a), but for PAC, NAM, ATL and EUR tracers respectively. f) The shadings are the model July to August climatological meridional wind (1981-1990) averaged from 800 to 200 hPa. Unit in m/s. The contours are the climatological zonal wind at the same vertical levels during the same time period. Contour interval is 5 m/s.
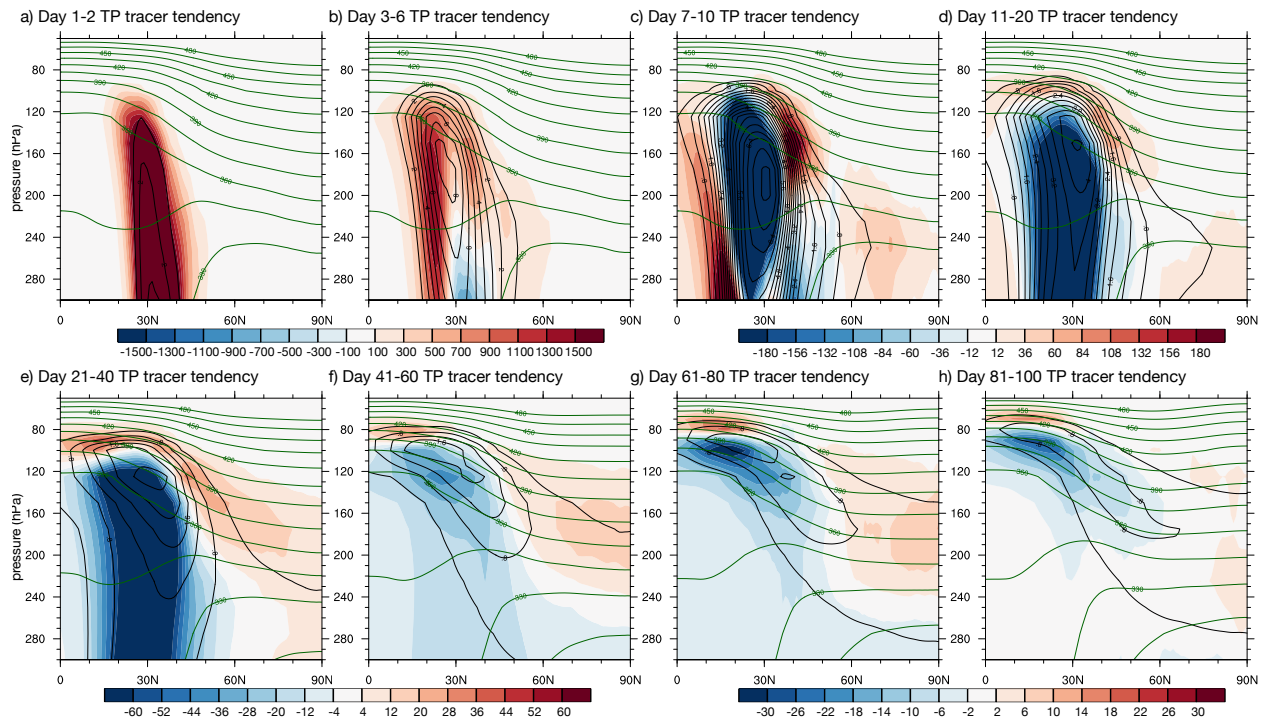
Figure 7. a) The shadings are zonally averaged tracer concentration tendency during day 1-2 for TP tracers. Unit in ppmv/day. The black contours are the zonally averaged tracer concentration. Contour interval is 0.5 millimole/mole. The green contours are the potential temperature levels. Contour interval is 15 K. b) The same as a) but for day 3-6. c)-h) The same as a), but for day 7-10, 11-20, 21-40, 41-60, 61-80 and 81-100 respectively. The tracer concentration contour (black) interval is 0.2 mmol/mol.

1014
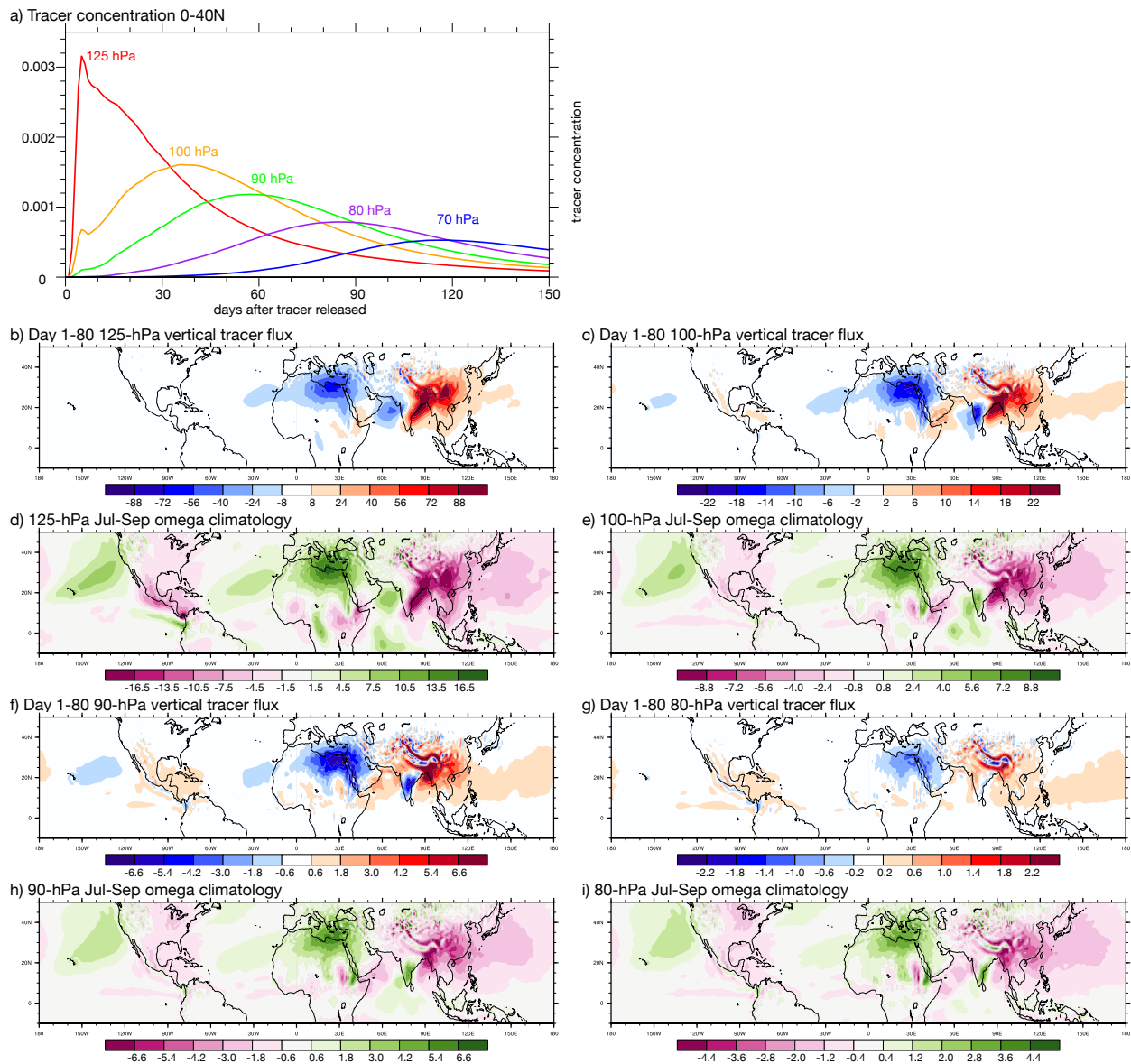
Figure 8. a) Temporal evolution of zonally averaged TP tracer concentration from 0-40°N for 125, 100, 90, 80 and 70 hPa. Unit in mol/mol. b) Vertical tracer flux averaged during day 1-80 at 125 hPa (red for upward flux and blue for downward flux). Unit in (mol/mol) · (m/s). c) The same as b) but for 100 hPa. d) Model July to September climatological vertical velocity (1981-1990). Unit in Pa/s. e) The same as d) but for 100 hPa. f)-g) The same as b), but for 90 and 80 hPa respectively. h)-i) The same as d) but for 90 and 80 hPa respectively.
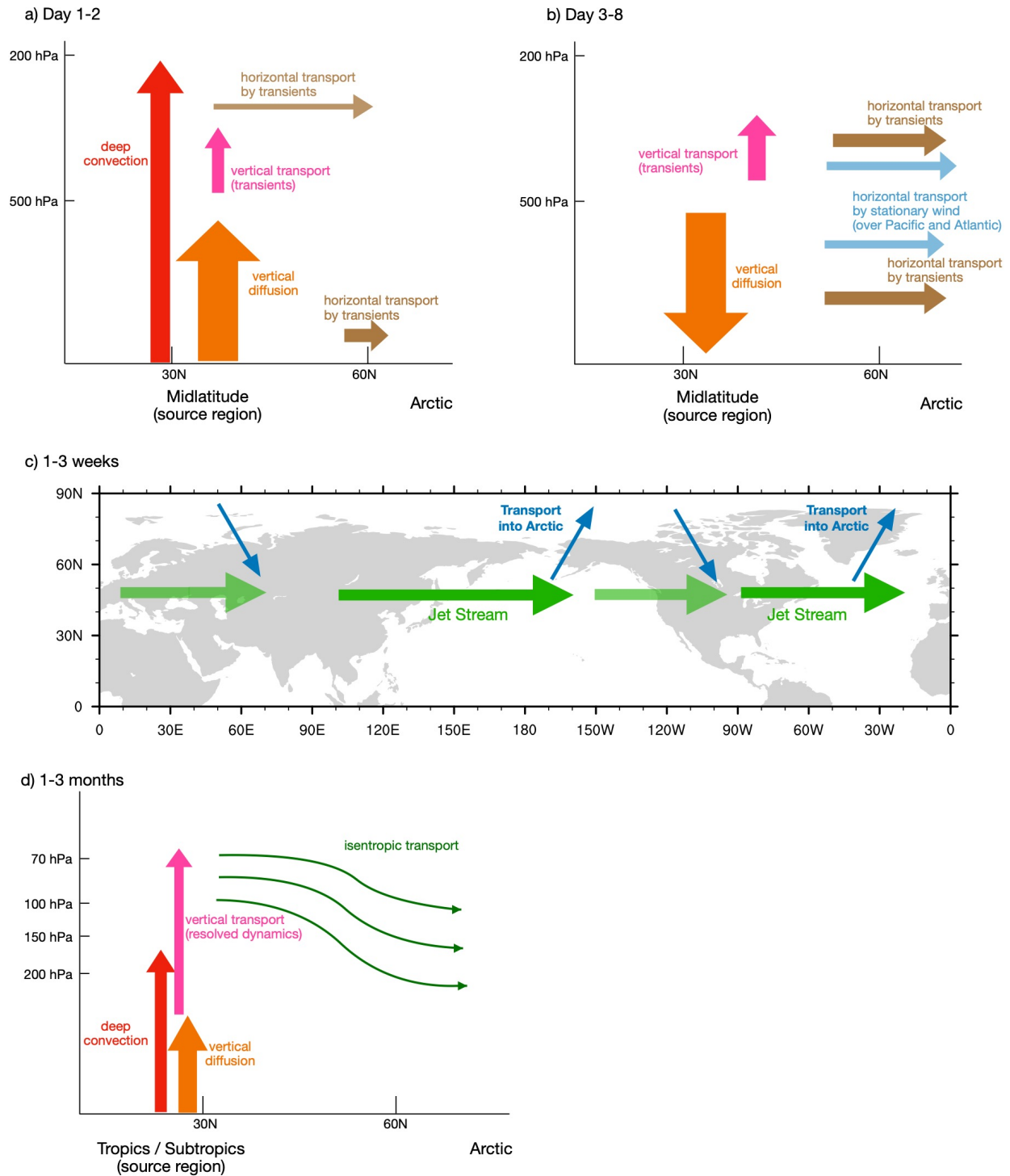
Figure 9. Schematic diagrams for different transport pathways. a)-b) The fast transport pathway. The width of the arrows indicates the relative importance of different processes. c) The intermediate transport pathway. d) The slow transport pathway.